Rare Variants in *BNC2* Are Implicated in Autosomal-Dominant Congenital Lower Urinary-Tract Obstruction

Caroline M. Kolvenbach,[1,2,3,28] Gabriel C. Dworschak,[1,2,4,28] Sandra Frese,[1,4] Anna S. Japp,[5] Peggy Schuster,[6] Nina Wenzlitschke,[6] Öznur Yilmaz,[2] Filipa M. Lopes,[7] Alexey Pryalukhin,[9] Luca Schierbaum,[1,4] Loes F.M. van der Zanden,[10] Franziska Kause,[1,3] Ronen Schneider,[3] Katarzyna Taranta-Janusz,[11] Maria Szczepańska,[12] Krzysztof Pawlaczyk,[13] William G. Newman,[8] Glenda M. Beaman,[8] Helen M. Stuart,[8] Raimondo M. Cervellione,[14] Wouter F.J. Feitz,[15] Iris A.L.M. van Rooij,[10,16] Michiel F. Schreuder,[17] Martijn Steffens,[18] Stefanie Weber,[19] Waltraut M. Merz,[20] Markus Feldkötter,[21] Bernd Hoppe,[21] Holger Thiele,[22] Janine Altmüller,[22,23] Christoph Berg,[20] Glen Kristiansen,[8] Michael Ludwig,[24] Heiko Reutter,[4,25] Adrian S. Woolf,[7] Friedhelm Hildebrandt,[3] Phillip Grote,[6] Marcin Zaniew,[26] Benjamin Odermatt,[2,27,28,*] and Alina C. Hilger[1,4,28,*]

Congenital lower urinary-tract obstruction (LUTO) is caused by anatomical blockage of the bladder outflow tract or by functional impairment of urinary voiding. About three out of 10,000 pregnancies are affected. Although several monogenic causes of functional obstruction have been defined, it is unknown whether congenital LUTO caused by anatomical blockage has a monogenic cause. Exome sequencing in a family with four affected individuals with anatomical blockage of the urethra identified a rare nonsense variant (c.2557C>T [p.Arg853*]) in *BNC2*, encoding basonuclin 2, tracking with LUTO over three generations. Re-sequencing *BNC2* in 697 individuals with LUTO revealed three further independent missense variants in three unrelated families. In human and mouse embryogenesis, basonuclin 2 was detected in lower urinary-tract rudiments. In zebrafish embryos, *bnc2* was expressed in the pronephric duct and cloaca, analogs of the mammalian lower urinary tract. Experimental knockdown of Bnc2 in zebrafish caused pronephric-outlet obstruction and cloacal dilatation, phenocopying human congenital LUTO. Collectively, these results support the conclusion that variants in *BNC2* are strongly implicated in LUTO etiology as a result of anatomical blockage.

Congenital lower urinary-tract obstruction (LUTO) generally manifests as urinary bladder outflow obstruction, which can represent an anatomical blockage or a functional obstruction. LUTO of any kind has an estimated birth prevalence of three per 10,000 pregnancies.[1] The largest population-based study from the West Midlands Congenital Anomaly Register in the UK suggests a significantly higher prevalence among black and minority ethnic groups than among white Europeans.[1]

Little is known about the genetic causes of anatomical LUTO. Single cases in the literature are associated with trisomy 21 or chromosomal aberrations, but for the majority of cases, the origin of isolated anatomical LUTO remains unknown. Functional LUTO has been extensively genetically

[1]Department of Pediatrics, Children's Hospital, University Hospital Bonn, 53113 Bonn, Germany; [2]Institute of Anatomy, University of Bonn, 53115 Bonn, Germany; [3]Division of Nephrology, Department of Medicine, Boston Children's Hospital, Harvard Medical School, Boston, MA 02115, United States; [4]Institute of Human Genetics, University of Bonn, 53127 Bonn, Germany; [5]Institute of Neuropathology, University of Bonn Medical Center, 53127 Bonn, Germany; [6]Institute of Cardiovascular Regeneration, Center for Molecular Medicine, Goethe University, 60439 Frankfurt am Main, Germany; [7]Division of Cell Matrix and Regenerative Medicine, School of Biological Sciences, Faculty of Biology, Medicine, and Health, University of Manchester, Manchester Academic Health Science Centere, Manchester M13 9PT, United Kingdom; [8]Division of Evolution and Genomic Sciences, School of Biological Sciences, Faculty of Biology, Medicine, and Health, University of Manchester, Manchester Academic Health Science Centre, Manchester M13 9PT, United Kingdom; [9]Institute of Pathology, University Hospital Bonn, 53127 Bonn, Germany; [10]Radboud Institute for Health Sciences, Department for Health Evidence, Radboud University Medical Center, 6525 GA Nijmegen, the Netherlands; [11]Department of Pediatrics and Nephrology, Medical University of Białystok, 15-089 Białystok, Poland; [12]Department and Clinics of Pediatrics, School of Medicine with the Division of Dentistry in Zabrze , Medical University of Silesia in Katowice, 40-055 Zabrze, Poland; [13]Department of Nephrology, Transplantology, and Internal Medicine, Poznan University of Medical Sciences, 61-701 Poznan, Poland; [14]Paediatric Urology, Royal Manchester Children's Hospital, Central Manchester University Hospitals NHS Foundation Trust, Manchester M13 9WL, United Kingdom; [15]Department of Urology, Pediatric Urology, Radboudumc Amalia Children's Hospital, 6525 GA Nijmegen, the Netherlands; [16]Department of Surgery–Pediatric Surgery, Radboudumc Amalia Children's Hospital, 6525 GA Nijmegen, the Netherlands; [17]Department of Pediatric Nephrology, Radboud University Medical Center, Radboud Institute for Molecular Life Sciences, Amalia Children's Hospital, 6525 GA Nijmegen, the Netherlands; [18]Department of Urology, Isala, 8025 AB Zwolle, the Netherlands; [19]Department of Pediatrics, University Hospital Marburg, 35037 Marburg, Germany; [20]Department of Obstetrics and Prenatal Medicine, University of Bonn, 53127 Bonn, Germany; [21]Division of Pediatric Nephrology, Department of Pediatrics, University Hospital Bonn, 53129 Bonn, Germany; [22]Cologne Center for Genomics, University of Cologne, 50391 Cologne, Germany; [23]Center for Molecular Medicine Cologne, University of Cologne, 50391 Cologne, Germany; [24]Department of Clinical Chemistry and Clinical Pharmacology, University of Bonn, 53127 Bonn, Germany; [25]Department of Neonatology and Pediatric Intensive Care, Children's Hospital, University of Bonn, 53127 Bonn, Germany; [26]Department of Pediatrics, University of Zielona Góra, 56-417 Zielona Góra, Poland; [27]Institute of Neuro-Anatomy, University of Bonn, 53115 Bonn, Germany
[28]These authors contributed equally
*Correspondence: b.odermatt@uni-bonn.de (B.O.), alina.hilger@uni-bonn.de (A.C.H.)
https://doi.org/10.1016/j.ajhg.2019.03.023.

Table 1. Heterozygous Variants of *BNC2* in Families With LUTO

Family	Family 1				Family 2			Family 3		Family 4	Family 5
Individual	IV-2	III-4	III-2	II-4	III-1	II-1	I-1	II-1	I-1	II-1	II-1
Sex	male	female	female	female	male	male	female	male	male	male	male
Phenotype	distal urethral stenosis, BL VUR grade 5	urethral stenosis, urinary tract infections, pollakisuria with nycturia	meatal urethral stenosis, bladder descensus, pollakisuria with nycturia, urinary incontinence	urethral stenosis	PUV, Rt VUR grade 5, BL renal hypodysplasia	pathological voiding on uroflowmetry	normal RUS and renal function	PUV, VUR grade 1-2.5, bladder diverticles	NA	PUV, right hydonephrosis,left VUR grade 1, incontinence until 6 years	PUV, VUR, ESRD
Age of clinical onset	13 weeks of gestation	12 years	47 years	42 years at surgical correction	prenatal	38 years at finding of pathological uroflowmetry	NA	7 years	NA	8 years	~11 years
Nucleotide change	c.2557C>T				c.2663A>G			c.473C>T		c.1036G>C	c.13G>A
Transcript	ENST00000418777				ENST00000380672			ENST00000380672		ENST00000380672	ENST00000545497
RefSeq	GenBank: NM_001317939.1				GenBank: NM_017637.6			GenBank: NM_017637.6		GenBank: NM_017637.6	NA
State	heterozygous				heterozygous			heterozygous		heterozygous	heterozygous
Chr. Pos. (GRCh37/hg19)	chr9: 16435054				chr9: 16419624			chr9: 16552724		chr9: 16437156	chr9: 16832274
Aminoacid change	p.Arg853*				p.His888Arg			p.Thr158Ile		p.Glu346Gln	p.Val5Ile
Conserved to	NA				drosophila melanogaster			danio rerio		danio rerio	pongo albelii
Protein domain	*not known*				*c2h2 zinc finger domain*			*not known*		*not known*	*not known*
GERP score	NA				5.59			5.84		5.96	-0.728
PPH (score)	NA				probably damaging (0.981)			possibly damaging (0.878)		benign (0.037)	benign (0.015)
SIFT (score)	NA				deleterious (0)			deleterious (0)		deleterious (0)	tolerated (0.59)
CADD score	19.09				25.7			26.6		22.1	1.466
ACMG	pathogenic				pathogenic			uncertain significance		uncertain significance	benign

(*Continued on next page*)

Table 1. *Continued*

Family	Family 1	Family 2	Family 3	Family 4	Family 5
rsNumber	rs1350162888	novel	rs144242525	rs945575406	rs750936655
gnomAD Allele Frequencies (hom/het/WT)	0.000028 (0/5/245862)	novel	0.000012 (0/3/245862)	0.000004 (0/1/245862)	0.000048 (0/6/124816)
ethnicity, gender	3 female AFR, 2 female NFE	novel	1 NFE male, 2 NFE female	1 NFE male	4 SAS, 1AMR, 1 ASJ, 4 female, 2 male

Complete pedigrees of identified families in which affected members have both the LUTO phenotype and rare variants in *BNC2* can be found in Figure S2.
Abbreviations are as follows: het, heterozygous; PPH, PolyPhen prediction score; BL, bilateral; ESRD, end-stage renal disease; PUV, posterior urethral valve; Rt, right; VUR, vesico ureteral reflux; RUS, renal ultrasound; NA, not available; ACMG, American College of Human Genetics Standards and Guidelines Classification as pathogenic, likely pathogenic, uncertain significance, likely benign or benign; NFE, non-Finnish European; SAS, south Asian; AMR, American; and ASJ, Ashkenazi Jewish.
Variants that were rated as pathogenic by the ACMG guidelines were annotated with a ClinVar Accession Number (ENST00000418777, c.2557C>T [p.Arg853*], ClinVar: SCV000891778; ENST00000380672, c.2663A>G [p.His888Arg], ClinVar: SCV000854630).

defined, e.g., variants of *CHRM3* (MIM: 118494) in prune-belly syndrome,[2] variants of *HPSE2* (MIM: 613469) and *LRIG2* (MIM: 608869) in urofacial syndrome,[3,4] and variants of *MYH11* (MIM: 160745) and *ACTG2* (MIM: 102545) in microcolon megabladder hypoperistalsis syndrome.[5,6] Anatomical congenital LUTO can also be familial, albeit with interfamilial phenotypic variability, even between identical twins.[7–9] Severe forms of LUTO are usually diagnosed prenatally on the basis of a distended bladder that fails to empty with dilatation of the upper urinary tract. However, milder forms manifest postnatally, often with recurrent urinary tract infections (UTI).[10] Severe forms cause oligohydramnios and are associated with dysplastic kidney malformations that can be secondary to LUTO.[11] This can be deduced because similar kidney disease occurs in ovine fetuses with surgically generated LUTO.[12] Indeed, LUTOs are the leading cause for end-stage renal disease (ESRD) in children.[13] The most common anatomical causes of LUTO are posterior urethral valves (PUVs) at the level of the prostatic urethra, a lesion unique to males.[14] Less common are anterior urethral valves, also called urethral atresia, that can occur in either sex.[11,15]

Here, we present evidence that monoallelic variants in *BNC2*, coding for basonuclin 2, are strongly implicated in isolated anatomical LUTO.

The study was conducted in adherence to the Declaration of Helsinki. The respective informed consent was obtained from the affected individuals or by proxies in the case of minors. The study was approved by the ethics committee of the medical faculty of the University of Bonn (No. 146/12) as well as by the respective ethics committees of the collaborating centers in Boston, Manchester, and Nijmegen (AGORA data and biobank). Human embryonic material, collected with maternal consent and ethical approval (REC 08/H0906/21+5), was sourced from the MRC-Wellcome Trust Human Developmental Biology Resource. Zebrafish and mice were kept according to national law and to general recommendations in our fish facility in Bonn, Germany and the mouse facility in Frankfurt, Germany, respectively.

We used exome sequencing in a previously unreported family (family 1; for a detailed description, see Supplemental Data and Table 1) whose affected members had autosomal-dominant LUTO of variable phenotypic expression (Figure 1C). The male index individual (IV-2) received vesicoamniotic shunting at 13 weeks of gestation as a result of early diagnosis of severe LUTO. Postnatally he was diagnosed with high-grade urethral stenosis. His mother (III-4) was diagnosed with urethral stenosis at the age of 16. Prior to her pregnancy with the index individual, she had two spontaneous abortions of unknown cause (Figure 1C). The maternal grandmother (II-4) was diagnosed with distal urethral stenosis (meatal stenosis) at the age of 47. Her sister (II-2) denied having voiding dysfunction but did not consent to any urological or genetic assessment. In accordance with the previously

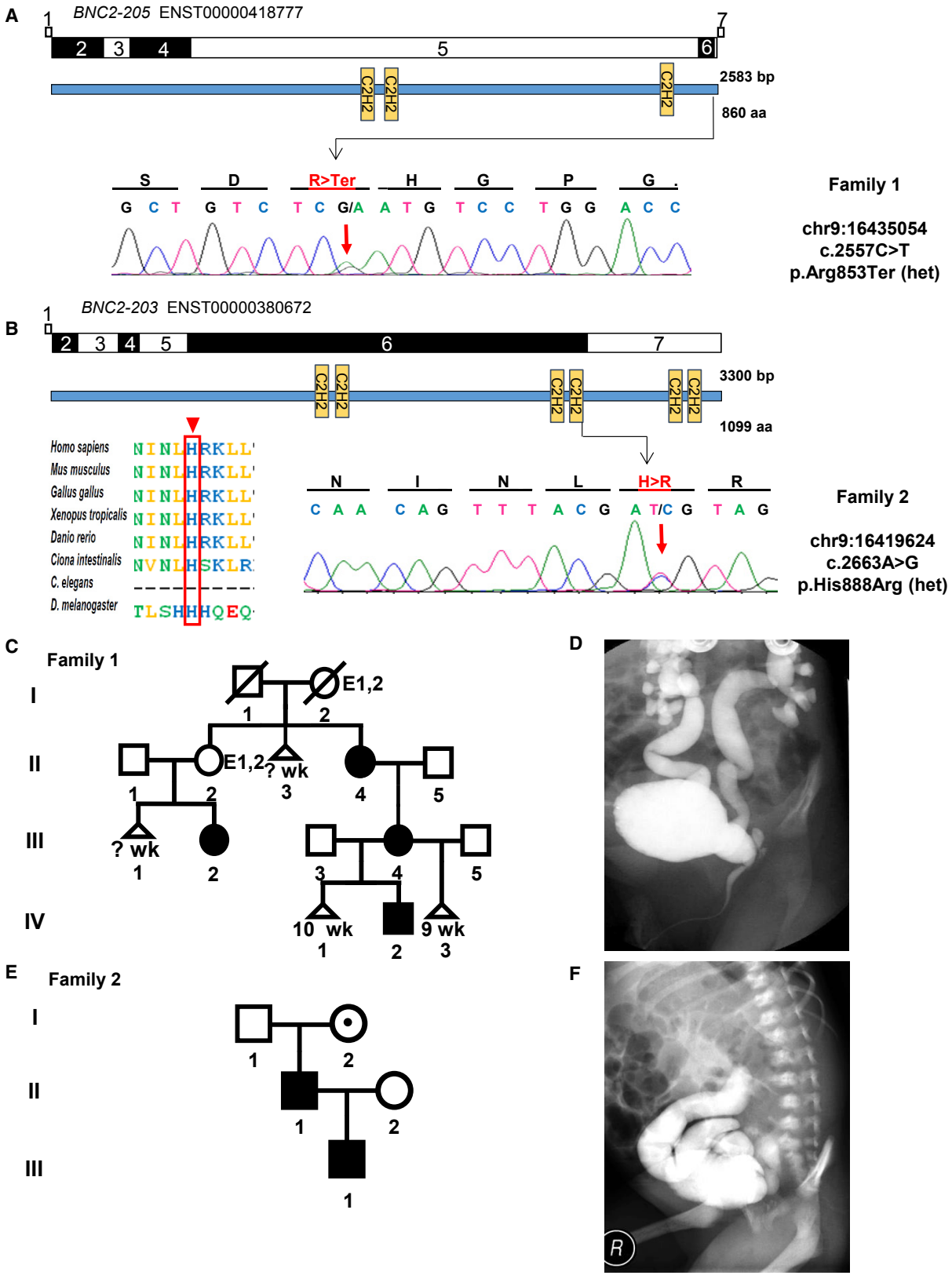

Figure 1. Exome Sequencing and Targeted Re-sequencing in Families with LUTO Phenotype Identifies Variants in *BNC2*
(A and B) Exon structures of *BNC2* cDNA of the two affected transcripts, ENST00000418777 and ENST00000380672, and protein domain structures are depicted. Positions of mutated nucleotides are indicated by arrows, and respective chromatograms are shown below. Evolutionary conservation among ortholog proteins is shown for family 2, carrying the p.His888Arg missense variant. The mutated amino acid residue is indicated with arrowheads and a red box. C2H2 = zinc-finger domain of the Cys2His2 folding group; *C. elegans* = *Caenorhabditis elegans* and *D. melanogaster* = *Drosophila melanogaster*.

(legend continued on next page)

described, well-noted, high within-family phenotypic variability, we considered her to be healthy. The female maternal cousin of the index individuals' mother (III-2) was diagnosed with high-grade urethral stenosis at the age of 42.

Exome sequencing was performed on the affected individuals, II-4, III-2, and IV-2 from family 1 (Figure 1C). According to recent reports on rare dominantly inherited congenital anomalies of the kidney and urinary tract (CAKUT), we considered only variants with an allele frequency <0.0001.[16,17] According to these filter criteria, we detected 11 missense and two nonsense variants that segregated in the family (Table S1). All variants were confirmed by Sanger sequencing. Among these variants, we prioritized the two nonsense variants as the most likely to be disease causing. One variant was found to be a novel p.Trp3* in *ALB* (MIM: 103600), encoding albumin. Recessive truncating variants in *ALB* have been described to cause analbuminaemia (MIM: 616000), whereas heterozygous variants in *ALB* can cause dysalbuminemic hyperthyroxinemia (MIM: 615999). Neither condition is associated with LUTO, and therefore the variant was not considered to be causative for the LUTO phenotype in the family. The second truncating variant, p.Arg853* rs1350162888 (ClinVar: SCV000891778) (total 860 amino acids) (Table 1), was found in *BNC2* (MIM: 608669, GenBank: NM_001317939, ENST00000418777) (Figure 1A), which is a candidate gene for human hypospadias and encodes basonuclin 2, a zinc-finger-containing protein.[18,19] Little is known about the function of BNC2. Previously, Vanhoutteghem et al. reported on the localization of BNC2 in nuclear speckles and its potential involvement in nuclear processing of mRNA.[20] Bhoj et al. analyzed *Bnc2* expression in the penis and urethra of $Bnc2^{+/-}$ and $Bnc2^{-/-}$ newborn mice and determined that *Bnc2* expression is highest in the phallic periurethral tissue,[18] consistent with *BNC2* having an important role in urethral development. They further suggested that *BNC2* acts locally in urethral development in both sexes. The variant in *BNC2* has been reported five times heterozygously in 175,684 alleles in the gnomAD database (version 2.0.2, date of inquiry 2018/09/20 for all mentioned gnomAD inquiries) (allele frequency 0.000028, rs1350162888). Notably, all of the heterozygous carriers were females.

We next re-sequenced all 14 *BNC2* transcripts in 697 individuals with LUTO from the AGORA study in the Netherlands and from pediatric nephrology departments in Germany, Poland, the UK, and the US. 13 of the 14 transcripts are predicted to be protein coding. The protein product for the two transcripts has been verified in humans so far (ENST00000380672, GenBank: NM_017637.6, canonical transcript; and ENST00000418777, GenBank: NM_001317939.1). In total, all rare missense or nonsense variants identified in this study were found in one of these two verified proteins except that one variant was identified in ENST00000545497. All variants identified in the canonical transcript ENST00000380672 are also contained by the alternatively spliced transcript ENST00000418777, in which the variant of family 1 was identified. By re-sequencing, we detected one novel (c.2663A>G [p.His888Arg], ENST00000380672, ClinVar: SCV000854630) and three rare missense variants (c.13G>A [p.Val5Ile], ENST00000545497, rs750936655, allele frequency 0.000048) (c.473C>T [p.Thr158Ile], ENST00000380672, rs144242525, allele frequency 0.000012) (c.1036G>C [p.Glu346Gln], ENST00000380672, rs945575406, allele frequency 0.000004) in four independent individuals with LUTO (Table 1, Figure S2). The novel variant c.2663A>G, detected in an individual with PUV and severe secondary dilatation of his upper urinary tract (III-1, family 2, Figure 1E), was inherited from an affected father (II-1) who had a pathological uroflowmetry (Figure S1). His renal ultrasound and renal function were normal. Investigation of the paternal grandparents (I-1 and I-2) showed that the variant was inherited from the healthy grandmother who did not have any history of UTI, pollakisuria, or nycturia and who had normal kidneys on renal ultrasound and normal uroflowmetry. The amino acid change p.His888Arg is highly conserved to *D. melanogaster* (GERP 5.59). Three *in silico* prediction programs classify the amino acid change as potentially disease causing and (according to the American College of Medical Genetics [ACMG] guidelines) as pathogenic (Table 1). The variant (c.2663A>G [p.His888Arg], ENST00000380672) is located in the fourth C2H2 zinc finger domain (Figure 1B). According to SwissProt entry Q6ZN30 and PROSITE, this variant is located near the second (residues 833–856) of three C2H2 zinc finger domains in BNC2 protein. However, InterPro and SMART include residue His888 in their signature matches (residues 833–856 and 861–888) for zinc-finger domains of the C2H2-type. These predictions suggest that this zinc finger's very last histidine, which is replaced by arginine,

(C) Pedigree with multiple affected individuals in the index family 1. Affection of individuals varies in severity: II-4—meatal stenosis, pollakisuria, and nycturia; III-2—urethral stenosis, surgically corrected, frequent UTI, pollakisuria, and nycturia; III-4—urethral stenosis, frequent UTIs in youth, pollakisuria, and nycturia; IV-2—prenatal diagnosis in 13th week of gestation with megacystis, urethral stenosis, surgically corrected and reconstructed. Individuals II-2 and I-2 are highlighted with the abbreviations E1 and E2 for unavailable genetic and clinical evaluation and represent potential *BNC2* carriers who did not participate in our study. Triangles denote miscarriages and are annotated with respective weeks of gestation. E1 = unavailable genetic evaluation; E2 = unavailable clinical evaluation; and Wk = week of gestation.
(D) Ventral micturation cystourethrogram (MCUG) image of affected individual IV-2; family 1 shows severe bilateral VUR grade V.
(E) Pedigree with multiple affected individuals of family 2. Carriers of the identified *BNC2* variant present with varying severity: I-2—no history of UTI or high voiding frequency, normal renal ultrasound; II-1—pollakisuria, nycturia, and pathological MCUG; and II-1—posterior urethral valve. I-2 is highlighted with a dot and represents a healthy carrier of the identified *BNC2* variant.
(F) Oblique MCUG image of affected individual III-2; family 2 shows severe right VUR grade V.

might interfere directly with the zinc finger domain's ability to bind to specific DNA sequences. Moreover, PROFAcc and ISIS, implemented in the PredictProtein server,[21,22] characterize His888 as an exposed residue, located in a protein-binding region. Because some C2H2 zinc-finger domains were also shown to facilitate binding to proteins or RNA,[23] the substitution p.His888Arg in BNC2 might affect not only DNA, but also RNA, and/or might target protein binding. Because this novel variant has been transmitted from an affected father to his affected son and because this variant resides in a highly conserved functional domain of BNC2, we believe this variant to be possibly disease causing (Table 1).

Of the remaining three rare missense variants detected in *BNC2*, the first variant, c.13G>A, detected in a boy with PUV and severe dilatation of his upper urinary tract (vesicoureteral reflux [VUR]) and secondary ESRD, has been reported in a heterozygous context six times (in two male and four female carriers) in 124,816 alleles according to gnomAD (allele frequency 0.000048). The GERP conservation score, the benign classification of three *in silico* prediction programs, and the ACMG guidelines suggest this variant to be benign. Parental DNA was not available for testing of inheritance (Table 1, family 5). The second rare missense variant, c.473C<T, detected in a male individual with PUV, has been mentioned in a heterozygous context three times (in one male and two female carriers) in 245,826 alleles according to gnomAD (allele frequency 0.000012). This variant is highly conserved and predicted by three *in silico* prediction programs to be disease causing. Because the variant was transmitted from a father with unknown affection status, we considered this variant to be a variant of unknown clinical significance (Table 1, family 3). The third rare missense variant, c.1036G>C, was detected in a male individual with PUV. It has been mentioned only once in a heterozygous context (in one male carrier) in 245,816 alleles according to gnomAD (allele frequency 0.000004). Although the amino acid at this position is highly conserved, only two out of three *in silico* prediction programs classified the variant to be disease causing. Parental DNA was not available for testing of inheritance (Table 1, family 4).

Hence, we classified the latter two missense variants, c.473C>T and c.1036G>C, each residing at a highly conserved amino acid position and predicted to be disease causing by at least two out of three *in silico* prediction programs according to the ACMG guidelines, as variants of unknown clinical significance. In addition to these four missense variants, we detected four rare (minor-allele frequency <0.0001) and two novel synonymous variants and one rare intronic variant (minor-allele frequency <0.0001) within the direct vicinity to the respective splice site (Table S2). The novel synonymous variant c.1132A>C (p.Ser358Ser) was predicted by four splice-site analysis programs to have an impact on splicing at this side (Table S2). Nevertheless, it remains speculative whether splicing is affected, and further assessment of this variant is warranted.

Thereafter we sought to characterize the embryonic effects on the contribution of *BNC2* to the formation of LUTO. *BNC2* encodes a highly conserved zinc-finger protein of poorly understood function. The Human Protein Atlas reports expression of BNC2 in the cytoplasm of urothelial cells of the bladder. To study the expression of *BNC2* in the human urethra, we performed immunohistochemistry staining with an anti-BNC2 antibody targeting a region in the N-terminal-vicinity third zinc finger of the canonical transcript ENST00000380672 (amino acids (aa) 661-787) and ENST00000418777 (aa 618–743). In a 7-week human embryo (Figure 2), BNC2 expression was detected in the urogenital sinus, the precursor of the bladder, and its outflow tract. The most prominent signal was in the primitive urothelium, and there was weaker immunoreactivity in the surrounding mesenchyme (Figure 2 A–D). Expression was also detected in the urothelium of the adult human male urethra (Figure S3). We performed expression analysis by *in situ* hybridization (ISH) in mouse embryos by using a *pan-Bnc2* probe that showed *Bnc2* expression in the developing lower urinary-tract structures, with emphasis on the genital tubercle (gt) above the phallic urethra and below the pelvic urethra at embryonic day (E) 13.5 (Figures 2E–2G), the critical time point for urethral development. Expression of *Bnc2* was also visible in the brain, in the mandibular region, and in dorsal parts above the spinal cord. The presence of the different *Bnc2* mRNA (Bnc2-201 and Bnc2-214) in the urogenital region of developing mouse embryos was verified by Sanger sequencing. These mouse mRNA represent the two different homologous human transcripts that were found to be affected by the variants identified in family 1 (ENST00000418777) and family 2 (ENST00000380672). Our expression data for *Bnc2* during murine development of the urinary tract and the existence of a heterozygous *Bnc2* knockout mouse, which was reported by Bhoij et al.[18] and presents with a cleft in the ventral part of the external genitalia, support the impact of *BNC2* in urethral development. Furthermore, Bhoij et al. describe homozygous knockout mice that have the same defect but in a more penetrant and severe form. These mice die soon after birth. Corresponding to that, the $Bnc2^{-/-}$ knockout mice, as described by Vanhoutteghem et al., die soon after birth. Because of their cleft palates and ingestion of air, these mice display aerial distention of their digestive tracts and therefore have distended abdomens.[24] The urinary tract was not examined in these mice, although a distended abdomen is also observed in human newborns with LUTO.[25]

In order to further investigate the function of *BNC2* during urinary tract development, we used zebrafish as a model organism. Their embryonic kidney, the pronephros, consists of two nephrons, with a fused glomerulus, two tubules, and ducts. The ducts terminate in a cloaca, altogether reflecting a simplified model of the human nephron and urinary tract.[26] BLAST analysis with human *BNC2* identified a single zebrafish *bnc2* ortholog

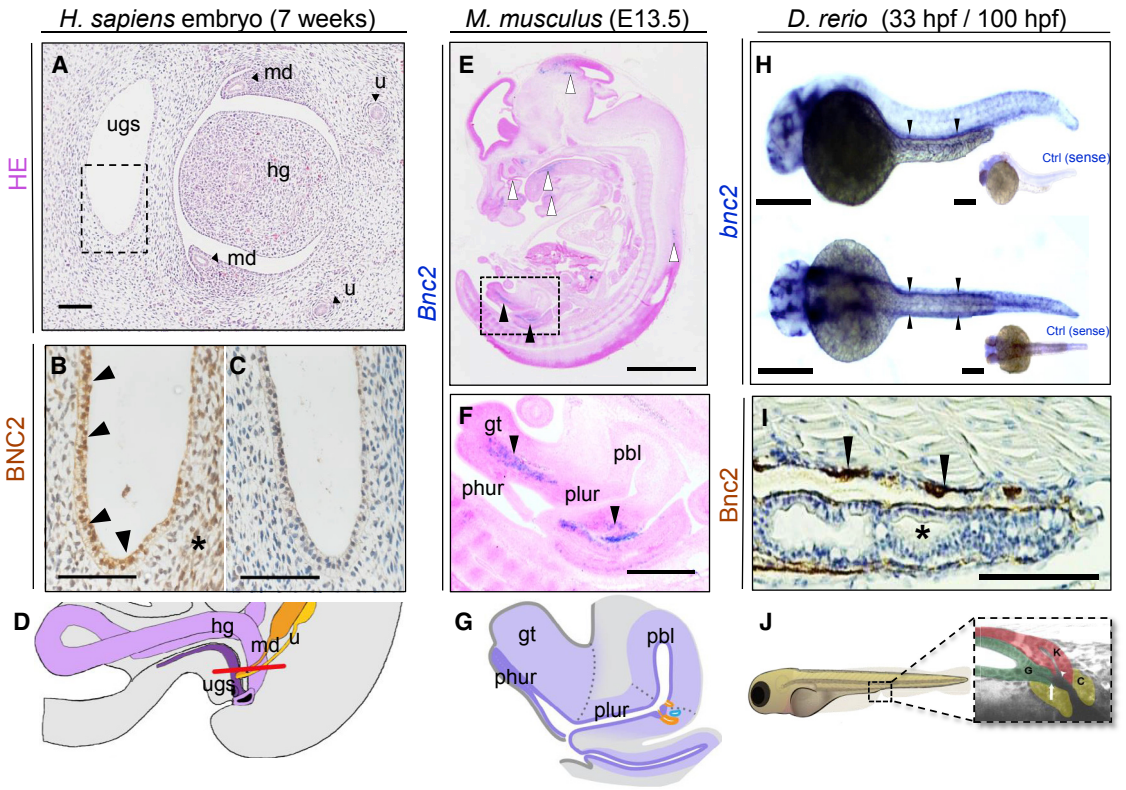

Figure 2. Embryonic Expression of *BNC2* in Human, Murine, and Zebrafish Larvae Urinary-Tract Tissue

(A) H&E-stained transverse section through a 7-week human embryo at the level of the urogenital sinus (ugs): the hindgut (hg), mesonephric ducts (md), and ureters (u) are also indicated. *H. sapiens* = *Homo sapiens*.

(B) Magnification of ugs, corresponding to the boxed region in (A), shows positive BCN2 immunoreactivity (brown) in the primitive epithelium (arrowheads) and adjacent mesenchyme (asterisk).

(C) There is only a faint background signal in this adjacent section in which the primary antibody was omitted.

(D) Schematic overview depicting the human embryonic anatomy of the cross-section in (A). A red line indicates a sectional plane.

(E and F) ISH with a *pan-Bnc2* probe on a sagittal section of a representative E13.5 (TS21) mouse embryo.

(E) *Bnc2* expression is visible (in blue) in the brain, in the mandibular region, and in a small patch at the dorsal side above the spinal cord (white arrowheads top to bottom). Specific expression is furthermore observed in the urogenital region (black arrowheads).

(F) Magnification (square in E) of the same embryo. Cells that express *Bnc2* are found in the gt above the phallic urethra (phur) and below the pelvic urethra (plur) (black arrowheads). M. musculus = *Mus musculus*; pbl = primitive bladder

(G) Schematic overview depicting the embryonic mouse anatomy of the cross-section in E.[39]

(H) Whole-mount ISH with an anti *bnc2* probe shows (in purple) the expression of *bnc2* RNA at 33 hpf in the pronephric ducts in WT zfl. In the lateral view (top), the pronephric duct is located above the yolk extension (black arrowheads), and in the dorsal view (bottom), the pairwise anlage of pronephric ducts are positively labeled. Sense controls (ctrl) did not show a staining. *D. rerio* = *Danio rerio*.

(I) Immunohistochemistry staining (in brown) against Bnc2 on a sagittal paraffin cross-section of WT zebrafish at 100 hpf indicates Bnc2-positive cells in the pronephric duct (black arrowheads) but not in the intestine (black asterisk).

(J) Schematic overview of pseudo-colored cloacal region of a 4 dpf zfl for better orientation and identification (modified according to Pyati et al.).[33] K = kidney (red); G = gut (green); and C = cloaca (yellow).

Scale bars represent 80 μm (A), 20 μm (B–C), 2 mm (E), 600 μm (F), 500 μm (H), and 100 μm (I)

encoding six different transcripts. To study the expression of *bnc2* in zebrafish larvae (zfl), we generated a labeled RNA probe for ISH. We detected strong expression of *bnc2* in the brain as described before[27] but also in the pronephric ducts and the developing cloaca region at 33 hours post-fertilization (hpf) (Figure 2H). Expression of Bnc2 in the pronephric ducts was confirmed by immunohistochemistry analysis in developing zfl at 100 hpf (Figure 2I, 2J).

Next, we performed phenotypic analysis after a Bnc2 knockdown in developing zfl. We designed one specific antisense Morpholino (MO), targeting the translation initiation site of transcript *bnc2_202* (ENSDART00000128671.4).

The canonical transcript in zebrafish *bnc2_202* (ZFIN and Ensembl genome browser) is the most similar to the two human *BNC2* transcripts that bear the discovered variants (ENST00000380672 and ENST00000418777). The zebrafish protein shows an amino acid similarity of 85%, similar protein structure, and a corresponding pattern of zinc-finger domains. The shorter 110 kDa version *bnc2_201* (ENSDART00000102322.6) is, as predicted, not targeted by the MO, as shown in the immunoblot analysis (Figure 3A).

Injecting embryos with 0.75 ng of *bnc2* MO caused a distal pronephric outlet obstruction, which is illustrated by a "vesicle" at the cloacal region. This "vesicle" was

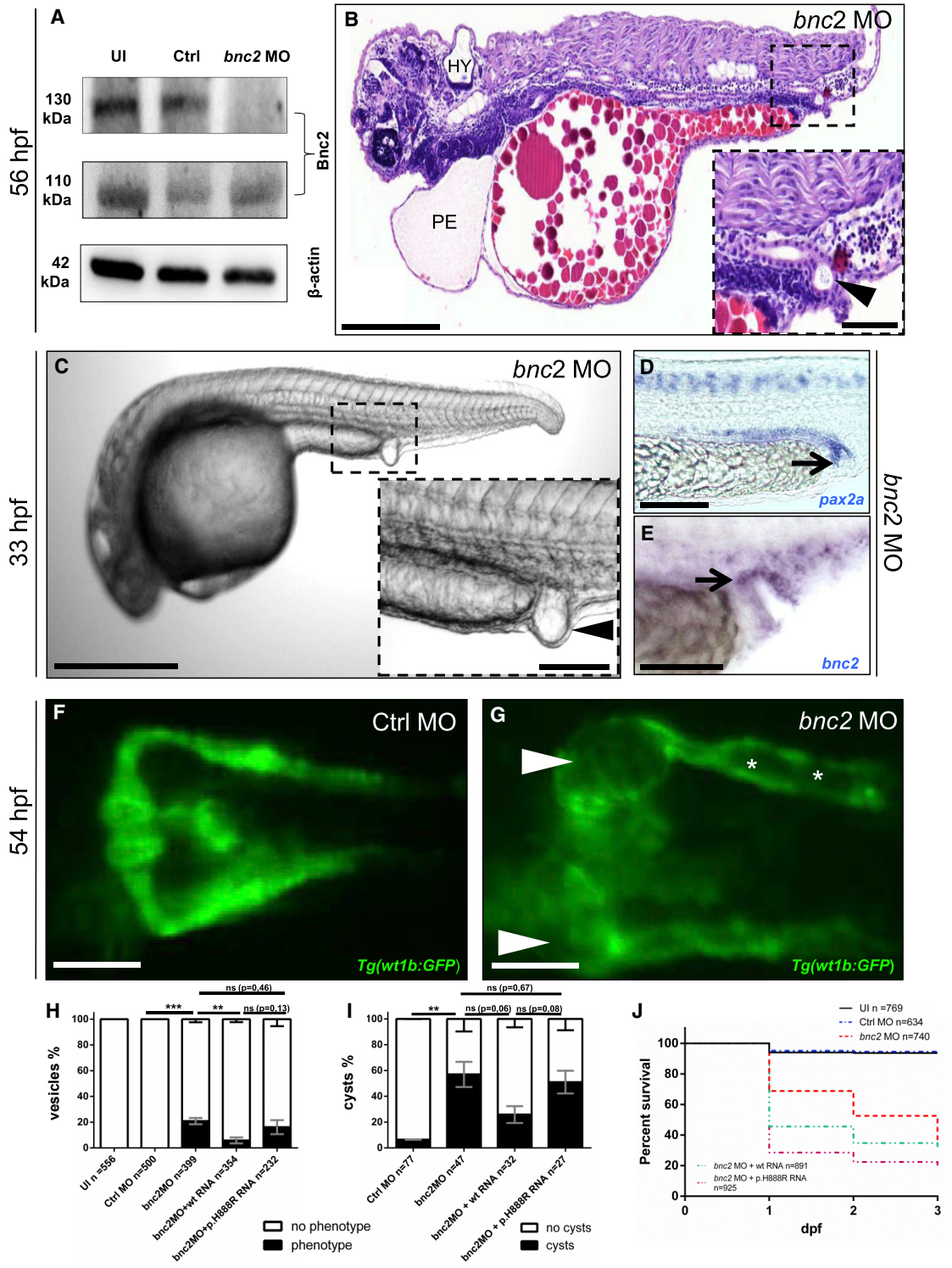

Figure 3. Depletion of Bnc2 Causes Pericardial Effusion, Hydrocephalus, Glomerular Cysts, and Distal Pronephric-Outlet Obstruction in Zebrafish

(A) Immunoblot analysis shows a protein decrease in *bnc2* MO-injected zfl for Bnc2-202 (130 kDa, C7DZJ6 according to UniProt ID) but not for Bnc2-201 (110 kDa, F1R42 according to UniProt ID) at 2 days dpf, which is as predicted for the specific MO target side. UI = uninjected.

(B) H&E staining of a sagittal section of a MO-injected zfl (lateral view, head to the left) shows (PE), hydrocephalus (HY), abnormal body curvature and a "vesicle" due to an outlet obstruction of the pronephric ducts (arrowhead in enlargement in B) at 56 hpf.

(C) Zfl injected with *bnc2* MO frequently develop a distal-outlet obstruction at 33 hpf; this obstruction is highlighted by an arrowhead in the enlargement of (C).

(D) Whole-mount ISH with a *pax2a* probe relates the constituent parts of the *bnc2* MO-induced pronephric-outlet obstruction to distal parts of the pronephric ducts and the cloacal region (black arrow).

(legend continued on next page)

detected in approximately 21% of *bnc2* MO-injected larvae at 33 hpf (n = 399) but in 0% in controls (n = 500, p = 0.0001 [unpaired t test]); these results resemble those for the anatomical blockage found in the human individuals with LUTO (Figures 3B, 3C, and 3H).

Besides this strikingly specific phenotype, the *bnc2* MO-injected zfl showed additional phenotypes such as abnormal body curvature (9%), hydrocephalus (HY) (5%), and pericardial effusion (PE) (44%). PE is sometimes considered to be nonspecific and is also seen in wild-type (WT) fish.[28] However, because of the high number of *bnc2* MO-injected zfl with PE, one might speculate that PE represents a secondary effect of kidney impairment. This has been described before in MO zebrafish experiments for monogenic nephrotic syndrome.[29] A previous study by Ogura et al. has shown abnormal body curvature in zfl overexpressing human *BNC2*; this abnormal curvature corresponds to a multifactorial etiology of human scoliosis.[30] The etiology of HY remains elusive; a relation to the pronephric defect seems unlikely.

To further study the involvement of Bnc2 in formation of the distal pronephric outlet obstruction, or dilatation, in the cloacal region (inlays in Figures 3B and 3C), we performed ISH in *bnc2* MO-injected zfl. A probe against *pax2a*, a marker for pronephric and cloacal tissue, indicated the intimate relation of the pronephric-outlet obstruction with the distal pronephric duct at the cloacal opening (Figure 3D). Because this MO only targets translation into Bnc2 protein and the expression of *bnc2* mRNA should not be altered, we could demonstrate *bnc2* expression overlapping with *pax2a* in the region of the pronephric-outlet obstruction (Figures 3D and 3E).

To assess the impact of the Bnc2 knockdown on the proximal pronephric ducts and the glomeruli, we used a transgenic *Tg(wt1b:GFP)* reporter fish, showing GFP expression in these tissues.[31] *bnc2* MO-injected *Tg(wt1b:GFP)* zfl demonstrated pronephric cysts at 54 hpf in 57% of survivors (n = 47) (Figures 3F–3G and 3J) but in 6.5% in controls (n = 77, p = 0.0067 [unpaired t test]). These cysts occur at the transition between neck and proximal convoluted tubule of the pronephric nephron. The formation of the pronephric cysts and dilated ducts is consistent with our hypothesis that a reduction of Bnc2 in zebrafish causes mechanical cloacal obstruction.

To demonstrate the specificity of the MO knockdown, we performed mRNA rescue experiments. Co-injection of *bnc2* MO together with human *BNC2* WT mRNA (transcript ENST00000380672, family 2) did not result in a reduction of the general mortality caused by the MO, but it could significantly rescue the LUTO-specific pronephric-outlet obstruction (Figures 3I and 3J) and furthermore reduce the MO-induced cysts in the *Tg(wt1b:GFP)* zfl (Figure 3H). To further prove the specificity of the observed LUTO-like phenotypes, we generated an independent transient CRISPR/Cas approach in which we designed single guide RNA (sgRNA) targeting different genomic positions in *bnc2*. sgRNA-6-injected zfl developed pronephric-foutlet obstruction similar to that developed by the *bnc2* MO-injected zfl at a rate of 5% at 33 hpf (n = 103) (Figure S4). Additionally, transient CRISPR/Cas Bnc2 knockdown larvae showed slight body curvature and HY for sgRNA 4 at 2 days post-fertilization (dpf) and a generally reduced survival rate similar to that of the *bnc2* MO zfl (Figure S4). This strongly suggested that the observed zebrafish phenotypes were caused by Bnc2 knockdown after administering *bnc2* MOs. Previously Lang et al., in an ENU-mutagenesis model, were able to show that bnc2$^{-/-}$KO zfl present with HY and adult zebrafish present with disturbed pigmentation.[27] In their study, the authors did not investigate their bnc2$^{-/-}$KO zfl for anomalies of the pronephric ducts or the cloacal region.

To assess the impact of the discovered alleles in *BNC2*, we compared two of these variants in the same MO rescue approach as described above but co-injected mRNA carrying the respective variants instead of WT mRNA. Co-injection of human *BNC2* mRNA bearing the p.His888Arg variant of family 2 did not result in a rescue of the pronephric outlet obstruction as observed with the WT mRNA (ENST00000380672) (Figure 3H). Consistently, co-injection of the same p.His888Arg *BNC2* mRNA failed to

(E) ISH with a *bnc2* probe in *bnc2* MO-injected embryos shows *bnc2* mRNA expression in relevant tissues forming a pronephric-outlet obstruction (black arrow).
(F and G) Zfl injected with *bnc2* MO develop glomerular cysts (white arrowheads in G) and dilatation of the pronephric ducts (white asterisk in G). Images from *in vivo* observation through fluorescence microscopy (dorsal view) in *Tg(wt1b:GFP)* were taken at 54 hpf in zfl injected with control (Ctrl) MO (F) and *bnc2* MO (G). *Tg* = transgenic zebrafish line.
(H) The graph shows 100% of all at 1 dpf surviving zfl of the five different cohorts: UI, Ctrl MO, *bnc2* MO, *bnc2* MO + WT human RNA, and *bnc2* MO + mutated human RNA (transcript ENST00000380672) bearing the p.His888Arg variant (for absolute numbers, see Figure 3H). A distal "vesicle" due to an outlet obstruction (phenotype) of the pronephric ducts can be seen in 21% of *bnc2* MO-injected zfl compared to 0% of zfl with a "vesicle" in both control groups ($p < 0.05$, unpaired t test). 6% of zfl injected with *bnc2* MO + WT mRNA develop a "vesicle," and so do 16% of zfl injected with *bnc2* MO + p.H888R. Data are presented as means with standard error of the mean (SEM).
(I) Quantification of glomerular cyst rates (phenotype) in *Tg(wt1b:GFP)* zfl at 2 dpf depicts significantly ($p < 0.05$, unpaired t test) clear glomerular cysts in 57% of *bnc2* MO-injected zfl. 26% of zfl injected with *bnc2* MO + WT RNA develop pronephric cysts; 51% of those injected with *bnc2* MO + p.His888Arg RNA develop pronephric *cysts*. Data are presented as means with SEM.
(J) Quantification of death rates at up to 3 dpf shows an increased mortality up to 64% in *bnc2* MO-injected zfl compared to zfl injected with UI (7%) and Ctrl MO (6%). With *bnc2* MO injected, zfl show significantly ($p < 0.0001$, Mantel-Cox test) reduced survival. Co-injection of *bnc2* MO + human WT RNA results in a mortality of 69%. Aggravated mortality up to 81% can be detected in the zfl injected with *bnc2* MO + p.His888Arg RNA.
Scale bars represent 200 μm (B), 50 μm (magnification in B), 500 μm (C), 100 μm (magnification in C), and 100 μm (D–G). **$p < 0.005$, *** $p < 0.0005$.

rescue the *bnc2*-MO-induced pronephric cysts in the *Tg(wt1b:GFP)* zfl (Figure 3I).

For the rescue experiments regarding the *BNC2* transcript ENST00000418777 affected in family 1, we observed a tendency toward a decrease of the distal pronephric-outlet obstruction. Co-injection of *BNC2* bearing the p.Arg853* variant showed no reduction of the specific phenotype (Figure S5).

The Bnc2 knockdown resulted in significantly reduced survival of zfl within 3 dpf (control [Ctrl] MO 94% versus *bnc2* MO 36%) (Figure 3J). Although the co-injection of human WT *BNC2* mRNA did not reduce mortality compared to that seen with solely *bnc2* MO injection (*bnc2* MO + WT RNA 69% [ENST00000380672]; *bnc2* MO + WT RNA 63% [ENST00000418777]), we observed a slightly aggravated mortality in zfl co-injected with mutated *BNC2* mRNA (*bnc2* MO + p.His888Arg RNA 81% [ENST00000380672]; *bnc2* MO + p.Arg853* RNA 88% [ENST00000418777]). We hypothesize several explanations for the failed rescue of mortality: general toxicity of mRNA, ubiquitous unregulated expression of BNC2, and the use of orthologous human mRNA in the zfl model. The distal pronephric-outlet obstruction is a very specific phenotype resembling the human LUTO phenotype, and because this obstruction can be rescued by human WT but not by mutated *BNC2* mRNA, the data clearly demonstrate the role of *BNC2* variants in LUTO.

We also employed an acute multi-sgRNA (mgRNA) approach targeting different positions in *bnc2*. This mgRNA resulted in median likelihoods of >99% for at least one variant on each allele deletion profiles, which were analyzed with the ICE synthego tool. We observed significantly reduced survival (50% median survival at 7 dpf) in zfl injected with *bnc2* mgRNA (sgRNA 2, 6, and 8) over a time period of 21 dpf in comparison to zfl injected with scrambled sgRNA (Ctrl) and uninjected larvae (UI) and 40% survival at the end of the experiment (Figure S1E). A distal-outlet obstruction of the pronephric ducts was detected in 3% of *bnc2*-mgRNA-injected embryos at 33 hpf (n = 35).

Our hypothesis that the "cloacal vesicle" is derived from pronephric tissue and represents a pronephric-outlet obstruction at the cloacal opening was supported by *bnc2* knockdown in the *mnr2b/hlxb9lb* enhancer trap line *Tg(HGj4A)*, which expresses GFP in the pronephric ducts during development.[32] Expression of GFP in cells lining the inner wall of the MO-induced pronephric-outlet obstruction clearly demonstrated that they belong to the distal pronephric duct (Figure 4A). High-resolution 3D stack imaging not only showed the connection of the pronephric ducts to the pronephric outlet obstruction but also exhibited dilatation of the distal part of the pronephric ducts (Figures 4B–4D). This finding is consistent with the observed dilatation of the proximal pronephric duct in the *Tg(wt1b:GFP)* line (Figure 3G, asterisks). Injecting a cell tracer dye, CellTracker Red CMTPX, into the pronephric-outlet obstruction at 33 hpf showed that the cells forming the "vesicle" become part of the distal pronephric duct and cloaca later in development (56 hpf and 74 hpf) as the pronephric-outlet obstruction eventually "ruptures" between 36 and 40 hpf (Figure S6).

In zebrafish, formation of the cloaca and opening occurs around 24–30 hpf through programmed cell death of epidermal cells.[33,34] Thus, we speculated that Bnc2, potentially acting as a transcription factor, controls the cell fate of the cloacal and pronephric-duct cells. Performing immunohistochemistry staining analysis with an anti-cleaved caspase 3 antibody, we detected a higher rate of apoptosis around the cloacal region and distal pronephric duct in *bnc2* MO zebrafish at 1 dpf and 2 dpf, suggesting that *bnc2* affects programmed cell death and leads to increased apoptosis (Figures 4E–G). One might speculate that the pronephric-outlet obstruction is causing retention of urine and that the resulting higher pressure in the pronephric ducts secondarily damages pronephric nephron cells and possibly the glomerular tissue and ultimately leads to cystic dilatation. However, the exact mechanism leading to the cloacal anomalies in *bnc2* MO-injected zfl remains elusive.

Several phenotypic features observed in *bnc2* MO-injected zfl (e.g., HY and cystic alterations of the kidneys) resemble features of the ciliopathy disease spectrum. Cells forming the pronephric duct normally exhibit multiple cilia that propel excreted urine toward the cloaca. Therefore, we were interested in determining whether cilia are morphologically altered in our knockdown morphants. Using immunofluorescence staining against acetylated tubulin and GFP in *Tg(wt1b:GFP)* zfl, we observed normal cilia morphology, but we also observed dilatation of the pronephric duct as observed previously in *bnc2* MO zfl at 56 hpf (Figures 4H and 4I).

Hence, after a Bnc2 knockdown in zfl, we observed phenotypic features resembling the human phenotypic LUTO spectrum. The pronephric-outlet obstruction reflects the anatomical blockage of human PUVs or urethral stenosis that leads to urine retention and consecutively to dilatation of proximal parts of the nephron. This dilatation could be demonstrated through the use of two transgenic lines. The pronephric cysts might resemble the kidney damage observed in human individuals with LUTO; such individuals often suffer from early-onset renal failure despite proper urine drain management.[35]

To assess the impact of the discovered variants p.His888Arg (family 2) and p.Arg853* (family 1), we performed mRNA rescue experiments. Co-injection of *bnc2* MO and human WT mRNA resulted in a reduction of the LUTO-specific phenotype, which could not be rescued by the respective mutated *BNC2* mRNA (Figure 3H–I, Figure S5). Thereby, we provided strong evidence for a pathogenic effect for the *BNC2* variants found in our index families (families 1 and 2).

The phenotypic spectrum of human LUTO phenotypes is broad and has displays interfamilial variability. Because milder forms can manifest at older ages, it must be assumed that within large control databases such as gnomAD, some

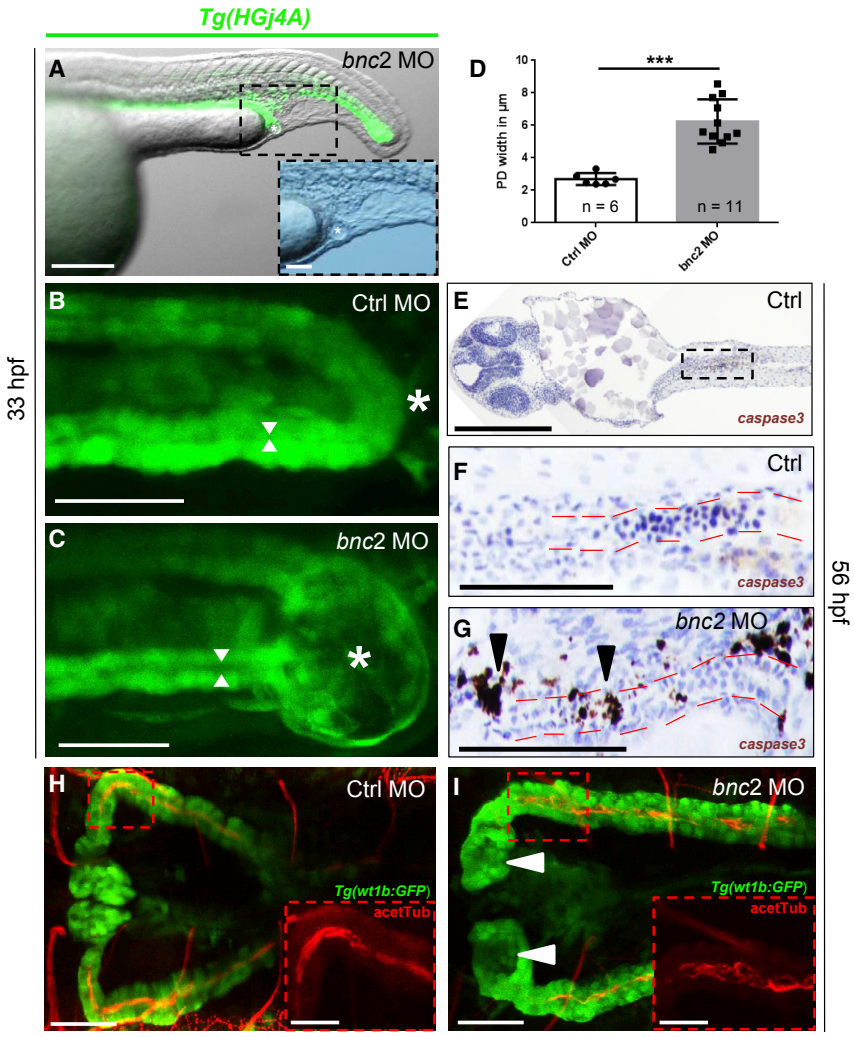

Figure 4. Distal Pronephric-Outlet Obstruction Is Formed by Pronephric Tissue and Causes Dilated Pronephric Ducts and Increased Apoptosis

(A) *Tg(HGj4A)* GFP-reporter zfl (lateral view) injected with *bnc2* MO emphasize the belonging of the distal pronephric-outlet obstruction, visible as a "vesicle" (marked with a white asterisk), to the distal pronephric duct and cloaca. The enlarged inlay shows the same "vesicle" in the sole bright-field image.

(B and C) High-resolution two-photon microscopy dorsal view of the cloacal region (white asterisks) in *Tg(HGj4A)* zfl injected with Ctrl MO (B) and *bnc2* MO (C) indicates the intimate relation of the pronephric-outlet obstruction to the bilateral pronephric ducts. Widths of the pronephric-duct lumen are indicated with white arrows.

(D) Quantification of pronephric-duct widths in *Tg(HGj4A)* zfl injected with *bnc2* MO shows significantly ($p = 0.0002$, Student's t test) dilated pronephric ducts compared to controls. PD = pronephric ducts. Data are presented as means with SEM.

(E–G) Cleaved caspase 3 staining in *bnc2* MO-injected zfl (56 hpf) shows an increased rate of apoptosis (black arrowheads in G) compared to Ctrl MO-injected embryos (E–F) around the pronephric duct (marked by red lines), the cloacal region, and the central nervous system (not shown). An overview emphasizing and localizing the pronephric regions shown in (F) and (G) is shown in €.

(H and I) Dorsal image from immunofluorescence staining of acetylated tubulin-stained cilia (red, acetTub) and GFP (green) depicts normal cilia morphology in the pronephric ducts in *Tg(wt1b:GFP)* zfl injected with Ctrl MO (H) and *bnc2* MO (I) at 56 hpf. Pronephric ducts are widened in the *bnc2* MO zfl as mentioned before. White arrowheads point to glomerular cysts in the *bnc2* MO zfl. The sole acetylated-tubulin stain (red channel) emphasizes cilia morphology in the respective enlargement inlays of (H) and (I).

Scale bars represent 200 µm (A), 50 µm (magnification of A–C), 100 µm (E–G), 50 µm (H and I), and 25 µm (magnifications of H and I). *** $p < 0.0005$.

individuals with a particular disease-causing variant or genotype fail to express most if not all features of the disease in question. This phenomenon is known as "reduced (or incomplete) penetrance."[36] Reduced penetrance is not uncommon; indeed, there are many known examples of "disease-causing variants" that fail to cause disease in a proportion of their carriers. As one example of such genes, *HNF1B* can be mentioned. Here, besides a variable phenotype even within families carrying the same variant, apparently unaffected family members could also be found to carry variants.[37] Reduced penetrance might therefore explain not only why monogenic diseases are occasionally transmitted through unaffected parents but also why healthy individuals can harbor quite large numbers of potentially disadvantageous variants in their genomes without suffering any clinically obvious phenotypes. Reduced penetrance can be a function of the specific variant(s) involved or of allele dosage.[38] It might also result from differential allelic expression, copy-number variation, or the modulating influence of independent genetic variants. The penetrance of some pathogenic genotypes is known to be age- and/or sex-dependent. Variable penetrance might also reflect the action of unlinked modifier genes, epigenetic changes, or environmental factors. Supporting this observation of incomplete penetrance in humans, our *bnc2* MO and CRISPR knockdown fish show a phenotypic spectrum ranging from pronephric cysts in 57% (in *bnc2* MO) to a visible pronephric-outlet obstruction ("vesicle") in 21% and 3%, respectively. Because PUVs, the most common human LUTO phenotype, are limited to males, one would expect to find a higher number of female than male carriers for monoallelic disease-causing variants among healthy control individuals. This circumstance might in part explain why all heterozygous carriers (n = 5) reported in gnomAD for the truncating variant p.Arg853* identified in our family 1 are females.

Functional studies in mouse embryos and our zfl studies now show that *BNC2* plays an important role in early

urinary-tract development across different species and suggest that *bnc2* deficiency in zfl causes pronephric-outlet obstruction and cystic anomalies of the pronephros and thereby phenocopies human LUTO. In conclusion, here we present evidence that monoallelic variants in BNC2, coding for basonuclin 2, are strongly implicated in human LUTO with anatomical blockage of the urethra.

Supplemental Data

Supplemental Data can be found online at https://doi.org/10.1016/j.ajhg.2019.03.023.

Acknowledgments

We thank affected individuals and their parents for participation in this study together with the German self-help organization for children with LUTO. We thank Mieczysław Litwin (The Children's Memorial Health Institute, Warsaw), Monika Miklaszewska, Katarzyna Zachwieja (Jagiellonian University, Cracow), Grażyna Krzemień, Agnieszka Szmigielska (Medical University of Warsaw), Marcin Tkaczyk, Daria Tomczyk (Polish Mothers Memorial Hospital Research Institute, Łódź), Przemysław Sikora (Medical University of Lublin)—all from Poland—for recruiting affected individuals. C.M.K. is supported by Scimed BONFOR grants O-149.0120 and O-167.0021. G.C.D. and A.C.H. are supported by BONFOR grants O-120.0001 and O-149.0123. H.R. and M.L. are supported by grants LU 731/3-1 and RE 1723/2-1 from the German Research Foundation (DFG). L.v.d.Z. is supported by the Dutch Kidney Foundation (Kolff grant No. 130OKJ36) and a ZonMW-VENI grant (016.186.036; the Netherlands Organisation for Scientific Research). F.H. is supported by the National Institutes of Health grant DK- 088767. N.W. is supported by DFG grant GR4745/1-1. P.S. and P.G. are supported by the DFG Excellence Cluster Cardio-Pulmonary System (Exc147-2). Purchase of the 2p microscope used in this study was supported by grant INST 1172/37-1 FUGG (DFG). Zebrafish work was supported by Bonn medical faculty zebrafish core facility. *Tg(wt1b:GFP)* zebrafish were provided by Christoph Englert and *Tg(HGj4A)* zebrafish by Koichi Kawakami. W.G.N., H.M.S., R.M.C., G.M.B., and A.S.W. are supported by grants from Kids Kidney Research and Newlife. F.M.L. and A.S.W. acknowledge support from Horizon 2020 Marie Skłodowska-Curie Actions RENALTRACT (942937). The MRC-Wellcome Trust Human Developmental Biology Resource provided human embryonic material.

Declaration of Interests

The authors declare no competing interests.

Received: September 21, 2018
Accepted: March 22, 2019
Published: May 2, 2019

Web Resources

Blood eQTL browser, https://www.genenetwork.nl/bloodeqtlbrowser/
ClinVar, https://www.ncbi.nlm.nih.gov/clinvar/
dbSNP build 135, https://www.ncbi.nlm.nih.gov/projects/SNP/
Ensembl database, http://www.ensembl.org/
German self-help organization for children with LUTO, http://www.luto-kinder.de/
GERP, http://mendel.stanford.edu/SidowLab/downloads/gerp/
gnomAD, https://gnomad.broadinstitute.org
GTEx Portal, https://www.gtexportal.org/home/
HaploReg v3, https://pubs.broadinstitute.org/mammals/haploreg/haploreg.php
ICE SYNTHEGO tool, https://ice.synthego.com/
MRC-Wellcome Trust Human Developmental Biology Resource, http://www.hdbr.org/
OMIM, http://omim.org/
PolyPhen, http://genetics.bwh.harvard.edu/pph2/
RegulomeDB, http://regulomedb.org/
SIFT, https://sift.bii.a-star.edu.sg/
SNP Annotation and Proxy search (SNAP, no longer available), https://www.broadinstitute.org/snap/snap/
T1Dbase, http://www.t1dbase.org
The Human Protein Atlas, https://www.proteinatlas.org/
Zfin, https://zfin.org/

References

1. Malin, G., Tonks, A.M., Morris, R.K., Gardosi, J., and Kilby, M.D. (2012). Congenital lower urinary tract obstruction: A population-based epidemiological study. BJOG *119*, 1455–1464.
2. Weber, S., Thiele, H., Mir, S., Toliat, M.R., Sozeri, B., Reutter, H., Draaken, M., Ludwig, M., Altmüller, J., Frommolt, P., et al. (2011). Muscarinic acetylcholine receptor M3 mutation causes urinary bladder disease and a prune-belly-like syndrome. Am. J. Hum. Genet. *89*, 668–674.
3. Daly, S.B., Urquhart, J.E., Hilton, E., McKenzie, E.A., Kammerer, R.A., Lewis, M., Kerr, B., Stuart, H., Donnai, D., Long, D.A., et al. (2010). Mutations in HPSE2 cause urofacial syndrome. Am. J. Hum. Genet. *86*, 963–969.
4. Stuart, H.M., Roberts, N.A., Hilton, E.N., McKenzie, E.A., Daly, S.B., Hadfield, K.D., Rahal, J.S., Gardiner, N.J., Tanley, S.W., Lewis, M.A., et al.; UK VUR Study Group; and 4C Study Group (2015). Urinary tract effects of HPSE2 mutations. J. Am. Soc. Nephrol. *26*, 797–804.
5. Gauthier, J., Ouled Amar Bencheikh, B., Hamdan, F.F., Harrison, S.M., Baker, L.A., Couture, F., Thiffault, I., Ouazzani, R., Samuels, M.E., Mitchell, G.A., et al. (2015). A homozygous loss-of-function variant in MYH11 in a case with megacystis-microcolon-intestinal hypoperistalsis syndrome. Eur. J. Hum. Genet. *23*, 1266–1268.
6. Wangler, M.F., Gonzaga-Jauregui, C., Gambin, T., Penney, S., Moss, T., Chopra, A., Probst, F.J., Xia, F., Yang, Y., Werlin, S., et al.; Baylor-Hopkins Center for Mendelian Genomics (2014). Heterozygous de novo and inherited mutations in the smooth muscle actin (ACTG2) gene underlie megacystis-microcolon-intestinal hypoperistalsis syndrome. PLoS Genet. *10*, e1004258.
7. Schreuder, M.F., van der Horst, H.J.R., Bökenkamp, A., Beckers, G.M.A., and van Wijk, J.A.E. (2008). Posterior urethral valves in three siblings: a case report and review of the literature. Birth Defects Res. A Clin. Mol. Teratol. *82*, 232–235.
8. Hanlon-Lundberg, K.M., Verp, M.S., and Loy, G. (1994). Posterior urethral valves in successive generations. Am. J. Perinatol. *11*, 37–39.
9. Frese, S., Weigert, A., Hoppe, B., Feldkötter, M., Ludwig, M., Weber, S., Kiliś-Pstrusińska, K., Zaniew, M., Reutter, H., and

Hilger, A.C. (2018). A classic twin study of lower urinary tract obstruction: Report of 3 cases and literature review. Low. Urin. Tract Symptoms *2018*, 17.
10. Scott, J.E. (1985). Management of congenital posterior urethral valves. Br. J. Urol. *57*, 71–77.
11. Dinneen, M.D., Dhillon, H.K., Ward, H.C., Duffy, P.G., and Ransley, P.G. (1993). Antenatal diagnosis of posterior urethral valves. Br. J. Urol. *72*, 364–369.
12. Farrugia, M.-K., Woolf, A.S., Fry, C.H., Peebles, D.M., Cuckow, P.M., and Godley, M.L. (2007). Radiotelemetered urodynamics of obstructed ovine fetal bladders: correlations with ex vivo cystometry and renal histopathology. BJU Int. *99*, 1517–1522.
13. Parkhouse, H.F., and Woodhouse, C.R. (1990). Long-term status of patients with posterior urethral valves. Urol. Clin. North Am. *17*, 373–378.
14. Robertson, W.B., and Hayes, J.A. (1969). Congenital diaphragmatic obstruction of the male posterior urethra. Br. J. Urol. *41*, 592–598.
15. Morris, R.K., and Kilby, M.D. (2011). Long-term renal and neurodevelopmental outcome in infants with LUTO, with and without fetal intervention. Early Hum. Dev. *87*, 607–610.
16. Vivante, A., Kleppa, M.-J., Schulz, J., Kohl, S., Sharma, A., Chen, J., Shril, S., Hwang, D.-Y., Weiss, A.-C., Kaminski, M.M., et al. (2015). Mutations in TBX18 cause dominant urinary tract malformations via transcriptional dysregulation of ureter development. Am. J. Hum. Genet. *97*, 291–301.
17. Sanna-Cherchi, S., Westland, R., Ghiggeri, G.M., and Gharavi, A.G. (2018). Genetic basis of human congenital anomalies of the kidney and urinary tract. J. Clin. Invest. *128*, 4–15.
18. Bhoj, E.J., Ramos, P., Baker, L.A., Garg, V., Cost, N., Nordenskjöld, A., Elder, F.F., Bleyl, S.B., Bowles, N.E., Arrington, C.B., et al. (2011). Human balanced translocation and mouse gene inactivation implicate Basonuclin 2 in distal urethral development. Eur. J. Hum. Genet. *19*, 540–546.
19. Kon, M., Suzuki, E., Dung, V.C., Hasegawa, Y., Mitsui, T., Muroya, K., Ueoka, K., Igarashi, N., Nagasaki, K., Oto, Y., et al. (2015). Molecular basis of non-syndromic hypospadias: systematic mutation screening and genome-wide copy-number analysis of 62 patients. Hum. Reprod. *30*, 499–506.
20. Vanhoutteghem, A., and Djian, P. (2006). Basonuclins 1 and 2, whose genes share a common origin, are proteins with widely different properties and functions. Proc. Natl. Acad. Sci. USA *103*, 12423–12428.
21. Rost, B., Yachdav, G., and Liu, J. (2004). The PredictProtein server. Nucleic Acids Res. *32*, W321-W326.
22. Ofran, Y., and Rost, B. (2007). ISIS: interaction sites identified from sequence. Bioinformatics *23*, e13–e16.
23. Brayer, K.J., Kulshreshtha, S., and Segal, D.J. (2008). The protein-binding potential of C2H2 zinc finger domains. Cell Biochem. Biophys. *51*, 9–19.
24. Vanhoutteghem, A., Maciejewski-Duval, A., Bouche, C., Delhomme, B., Hervé, F., Daubigney, F., Soubigou, G., Araki, M., Araki, K., Yamamura, K., and Djian, P. (2009). Basonuclin 2 has a function in the multiplication of embryonic craniofacial mesenchymal cells and is orthologous to disco proteins. Proc. Natl. Acad. Sci. USA *106*, 14432–14437.
25. Docimo, S.G., Canning, D., Khoury, A., and Salle, J.L.P. (2018). The Kelalis–King–Belman Textbook of Clinical Pediatric Urology (CRC Press).
26. Drummond, I.A., Majumdar, A., Hentschel, H., Elger, M., Solnica-Krezel, L., Schier, A.F., Neuhauss, S.C., Stemple, D.L., Zwartkruis, F., Rangini, Z., et al. (1998). Early development of the zebrafish pronephros and analysis of mutations affecting pronephric function. Development *125*, 4655–4667.
27. Lang, M.R., Patterson, L.B., Gordon, T.N., Johnson, S.L., and Parichy, D.M. (2009). Basonuclin-2 requirements for zebrafish adult pigment pattern development and female fertility. PLoS Genet. *5*, e1000744.
28. Hanke, N., Staggs, L., Schroder, P., Litteral, J., Fleig, S., Kaufeld, J., Pauli, C., Haller, H., and Schiffer, M. (2013). "Zebrafishing" for novel genes relevant to the glomerular filtration barrier. BioMed Res. Int. *2013*, 658270.
29. Gee, H.Y., Ashraf, S., Wan, X., Vega-Warner, V., Esteve-Rudd, J., Lovric, S., Fang, H., Hurd, T.W., Sadowski, C.E., Allen, S.J., et al. (2014). Mutations in EMP2 cause childhood-onset nephrotic syndrome. Am. J. Hum. Genet. *94*, 884–890.
30. Ogura, Y., Kou, I., Miura, S., Takahashi, A., Xu, L., Takeda, K., Takahashi, Y., Kono, K., Kawakami, N., Uno, K., et al. (2015). A functional SNP in BNC2 is associated with adolescent idiopathic scoliosis. Am. J. Hum. Genet. *97*, 337–342.
31. Perner, B., Englert, C., and Bollig, F. (2007). The Wilms tumor genes wt1a and wt1b control different steps during formation of the zebrafish pronephros. Dev. Biol. *309*, 87–96.
32. Asakawa, K., Abe, G., and Kawakami, K. (2013). Cellular dissection of the spinal cord motor column by BAC transgenesis and gene trapping in zebrafish. Front. Neural Circuits *7*, 100.
33. Pyati, U.J., Cooper, M.S., Davidson, A.J., Nechiporuk, A., and Kimelman, D. (2006). Sustained Bmp signaling is essential for cloaca development in zebrafish. Development *133*, 2275–2284.
34. Stickney, H.L., Imai, Y., Draper, B., Moens, C., and Talbot, W.S. (2007). Zebrafish bmp4 functions during late gastrulation to specify ventroposterior cell fates. Dev. Biol. *310*, 71–84.
35. Kilby, M.D., Somerset, D.A., and Khan, K.S. (2004). Potential for correction of fetal obstructive uropathy: time for a randomized, controlled trial? Ultrasound Obstet. Gynecol. *23*, 527–530.
36. Cooper, D.N., Krawczak, M., Polychronakos, C., Tyler-Smith, C., and Kehrer-Sawatzki, H. (2013). Where genotype is not predictive of phenotype: towards an understanding of the molecular basis of reduced penetrance in human inherited disease. Hum. Genet. *132*, 1077–1130.
37. Faguer, S., Decramer, S., Chassaing, N., Bellanné-Chantelot, C., Calvas, P., Beaufils, S., Bessenay, L., Lengelé, J.-P., Dahan, K., Ronco, P., et al. (2011). Diagnosis, management, and prognosis of HNF1B nephropathy in adulthood. Kidney Int. *80*, 768–776.
38. Basel-Vanagaite, L., Pelet, A., Steiner, Z., Munnich, A., Rozenbach, Y., Shohat, M., and Lyonnet, S. (2007). Allele dosage-dependent penetrance of RET proto-oncogene in an Israeli-Arab inbred family segregating Hirschsprung disease. Eur. J. Hum. Genet. *15*, 242–245.
39. Georgas, K.M., Armstrong, J., Keast, J.R., Larkins, C.E., McHugh, K.M., Southard-Smith, E.M., Cohn, M.J., Batourina, E., Dan, H., Schneider, K., et al. (2015). An illustrated anatomical ontology of the developing mouse lower urogenital tract. Development *142*, 1893–1908.

The American Journal of Human Genetics, Volume *104*

Supplemental Data

Rare Variants in *BNC2* Are Implicated in Autosomal-Dominant Congenital Lower Urinary-Tract Obstruction

Caroline M. Kolvenbach, Gabriel C. Dworschak, Sandra Frese, Anna S. Japp, Peggy Schuster, Nina Wenzlitschke, Öznur Yilmaz, Filipa M. Lopes, Alexey Pryalukhin, Luca Schierbaum, Loes F.M. van der Zanden, Franziska Kause, Ronen Schneider, Katarzyna Taranta-Janusz, Maria Szczepańska, Krzysztof Pawlaczyk, William G. Newman, Glenda M. Beaman, Helen M. Stuart, Raimondo M. Cervellione, Wouter F.J. Feitz, Iris A.L.M. van Rooij, Michiel F. Schreuder, Martijn Steffens, Stefanie Weber, Waltraut M. Merz, Markus Feldkötter, Bernd Hoppe, Holger Thiele, Janine Altmüller, Christoph Berg, Glen Kristiansen, Michael Ludwig, Heiko Reutter, Adrian S. Woolf, Friedhelm Hildebrandt, Phillip Grote, Marcin Zaniew, Benjamin Odermatt, and Alina C. Hilger

Supplemental note: Case report of Family 1

The male index individual (IV-2) was born spontaneously after preterm labor at 32+1 weeks of gestation to a 39-year-old gravida 3, para 0 mother, following a pregnancy complicated by early diagnosis of severe LUTO at 13 weeks of gestation. In order to prevent intrauterine renal insufficiency, vesicoamniotic shunting was performed directly after prenatal diagnosis at 13 weeks of gestation. Postnatal micturition cystourethrography at three weeks of life showed severe urethral obstruction suggesting PUV (Figure 1 **D**). Later surgical reconstruction with creation of a tubularized neourethra at nine months of age revealed the final diagnosis of urethral stenosis. The mother of the index individual (III-4) had a history of recurrent urinary tract infections starting at 12 years of age. In addition, she had early onset of increased urinary daytime frequency and nocturia with up to eight times per night. Urological workup at the age of 16 years including urodynamic testing revealed an underlying urethral stenosis. She rejected therapeutic urethral bouginages leaving her with a persistent increased urinary daytime frequency and nocturia at the time of assessment. Her first two pregnancies ended at nine and ten weeks of gestation respectively with spontaneous abortion of unknown cause (Figure 1 **C**). At the time of assessment, the maternal grandmother (II-4) of the index individual was 65 years. She also had an increased urinary daytime frequency and nocturia of up to five times per night. At 47 years she started to have urinary incontinence. Urological workup at that age revealed slight descensus of her bladder and distal urethral stenosis (meatal stenosis). The sister of the maternal grandmother (II-2) was 72 years of age at the time of assessment. She had one spontaneous abortion at nine weeks of gestation. She denied having voiding dysfunction but did not consent to any urological or genetic

assessment. In accordance with the previously described well-noted high within-family phenotypic variability, we considered her to be healthy. In contrast, her 43 year old daughter (III-2), had a history of early onset increased urinary daytime frequency and nocturia with urinary tract infections in her youth and was finally diagnosed with high grade urethral stenosis at 42 years of age which was surgically corrected at that time. Of note, the maternal great-grandmother (I-2) of the index individual (IV-2), had one spontaneous abortion at eight weeks of gestation and two living daughters (II-2 and II-4).

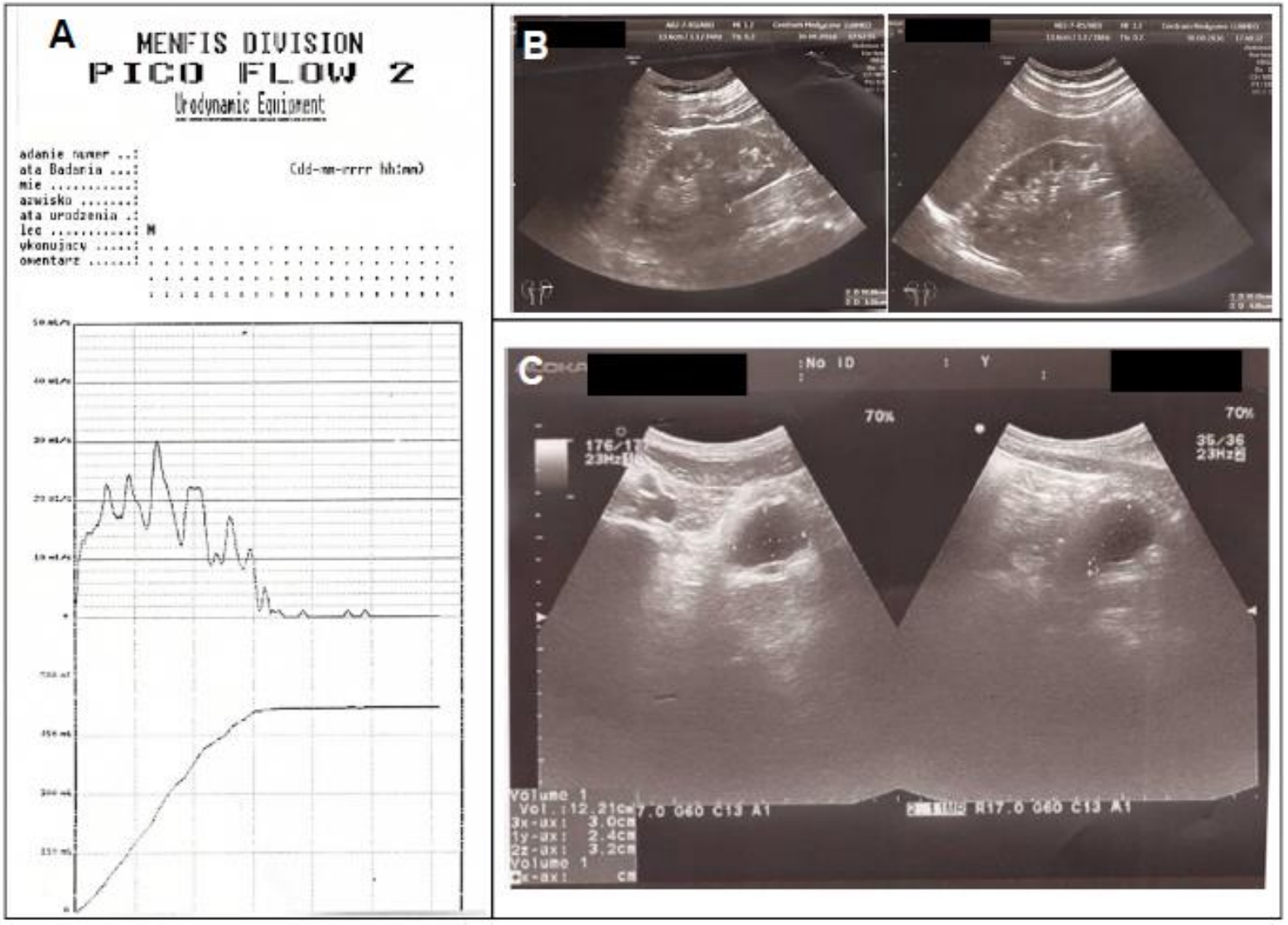
A
MENFIS DIVISION
PICO FLOW 2
Urodynamic Equipment
adanie numer ..:
ata Badania ...:
(dd-mm-rrrr hh:mm)
mie .....:
azwisko .....:
ata urodzenia .:
lec .....: M
ykonujacy .....:
omentarz .....:
B
C
:No ID
:
Y
70%
70%
35/36
23Hz
Volume 1
Vol.:12.21cm
3x-ax: 3.0cm
1y-ax: 2.4cm
2z-ax: 3.2cm
Volume 1
R17.0 060 C13 A1

Figure S1: Pathological Uroflowmetry of Individual II-1 in Family 2

(**A**): Uroflowmetry showing dysfunctional voiding, voided urine volume = 520 ml.

(**B**): Normal renal ultrasound of right and left kidney.

(**C**): Ultrasound of bladder showing 12 ml of residual urine after uroflowmetry.

A **Family 1** (c.2557C>T, p.R853*, ENST00000418777)

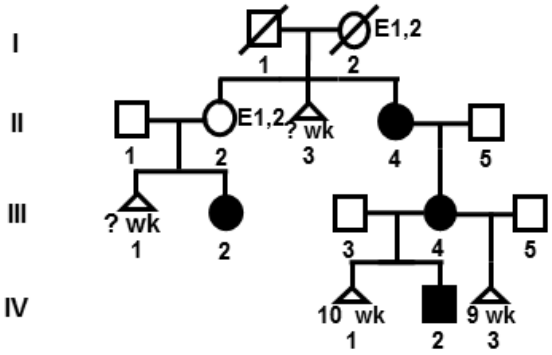

B **Family 2** (c.2663A>G, p.H888R, ENST00000380672)

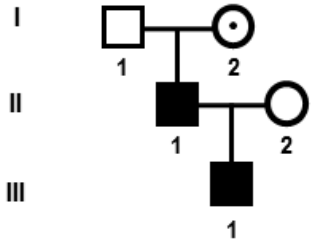

C **Family 3** (c.473C>T, p.T158I, ENST00000380672)

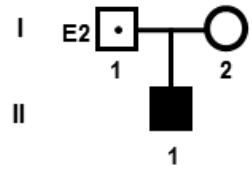

D **Family 4** (c.1036G>C, p.E346Q, ENST00000380672)

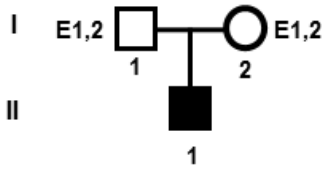

E **Family 5** (c.13G>A, p.V51I, ENST00000545497)

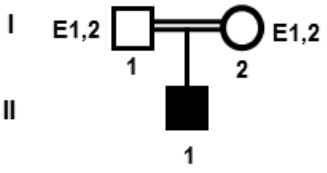

Figure S2: Pedigrees of Identified Families with LUTO Phenotype with Rare Variants in *BNC2*

(A): Pedigree with multiple affected individuals in the index Family 1. Affection of Individuals varies in severity: II-4: meatal stenosis, pollakisuria and nycturia; III-2: urethral stenosis, surgically corrected, frequent urinary tract infections (UTI), pollakisuria and nycturia; III-4: urethral stenosis, frequent UTIs in youth, pollakisuria and nycturia; IV-2: prenatal diagnosis in 13th week of gestation with megacystis, urethral stenosis, surgically corrected/reconstructed. Individuals II-2 and I-2 are more precisely highlighted with the symbol E1,2 for unavailable genetic and clinical evaluation, representing potential carriers of the *BNC2* variant but did not participate in our study. Triangles denote miscarriages and are annotated with respective weeks of gestation. E1 = unavailable genetic evaluation; E2 = unavailable clinical evaluation; Wk = week of gestation

(B): Pedigree with multiple affected individuals of Family 2. Carriers of the identified *BNC2* variant present with varying severity: I-2 no history of UTI or high voiding frequency, normal renal ultrasound; II-1: pollakisuria, nycturia and pathological MCUG; II-1: posterior urethral valve. I-2 is highlighted with a dot, representing a healthy carrier of the identified *BNC2* variant.

(C): Pedigree with one affected individual of Family 3. II-1 with the identified *BNC2* variant presents with posterior urethral valves, vesico ureteral reflux grade 1-2.5, bladder diverticles. I-1 is a carrier of the same variant, but was unavailable for clinical evaluation (E2).

(D): Pedigree with one affected individual of Family 4. II-1 with the identified *BNC2* variant presents with posterior urethral valves, right hydronephrosis, left vesico ureteral reflux

grade 1, incontinence until 6 years of age. The parents I-1 and I-2 were unavailable for genetic and clinical evaluation (E1,2).

(E): Pedigree with one affected individual of Family 5. II-1 from a consanguineous descent with the identified *BNC2* variant presents with posterior urethral valves, vesico ureteral reflux, end stage renal disease. The parents I-1 and I-2 were unavailable for genetic and clinical evaluation (E1,2).

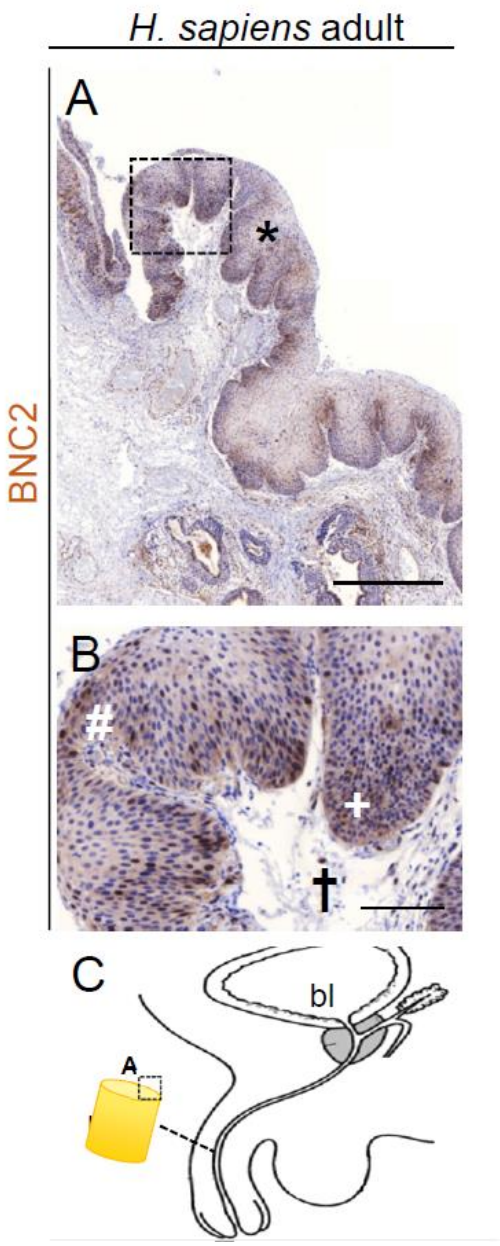
H. sapiens adult
BNC2
A
*
B
#
+
†
C
bl
A

Figure S3: Expression of Human BNC2 in Adult Male Urethra

(**A-B**): Immunohistochemistry staining for BNC2 on a transverse section of adult human distal urethra (positive stained tissue is marked with an asterisk *). (B) Magnification (square in A) of the basal layer of the squamous mucosa epithelium shows a weak cytoplasmic positive reaction with the antibody against BNC2 (+). Furthermore, a diffuse nuclear staining in all layers of the epithelium can be observed (#). In the stroma are some plasma cells with a positive staining (†).

(**C**): Schematic overview of the human male urogenital organ depicting the location of tissue (dashed square) shown in A. bl = bladder, peur =penile urethra.

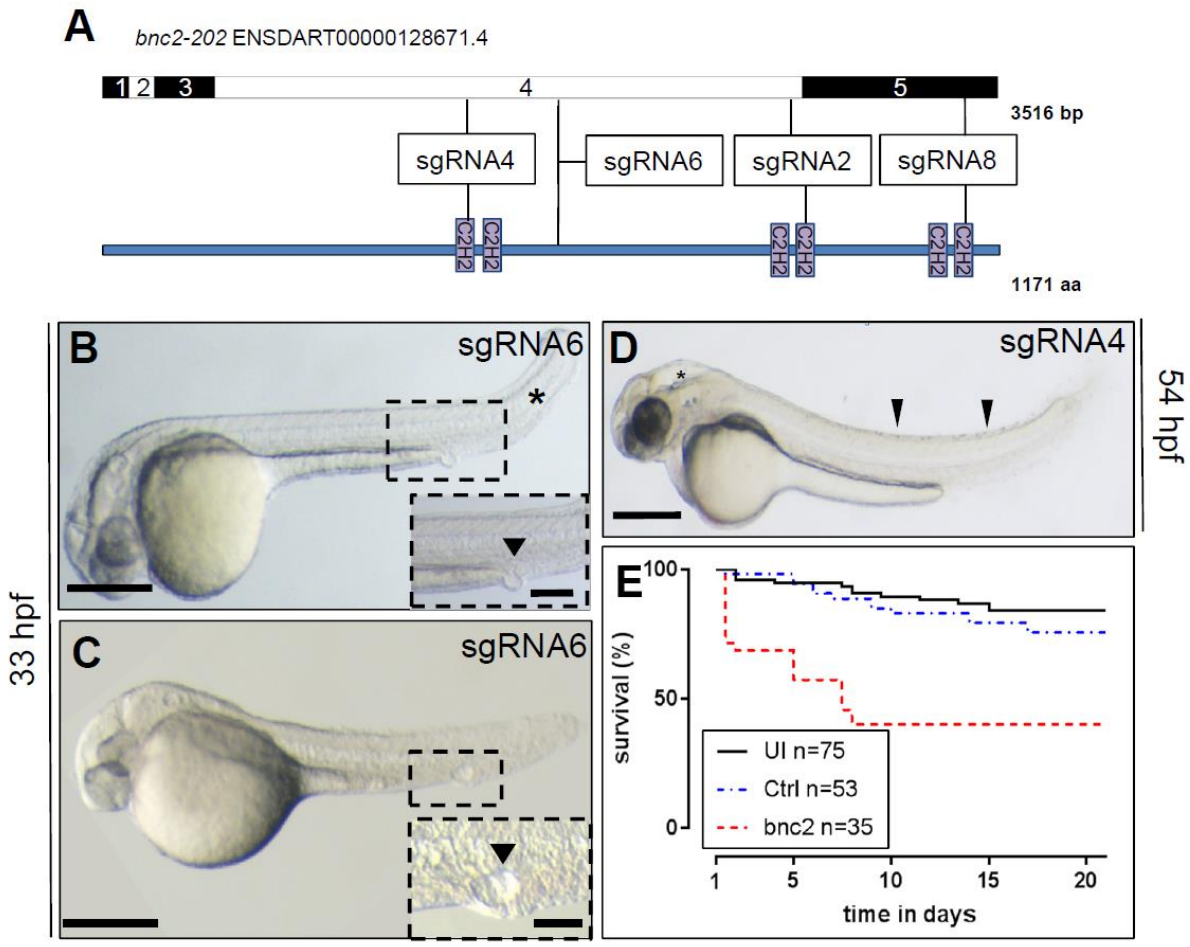
A
bnc2-202 ENSDART00000128671.4
1 2 3 4 5
3516 bp
sgRNA4
sgRNA6
sgRNA2
sgRNA8
C2H2
1171 aa
B
sgRNA6
C
sgRNA6
D
sgRNA4
54 hpf
33 hpf
E
survival (%)
100
50
0
UI n=75
Ctrl n=53
bnc2 n=35
1
5
10
15
20
time in days

Figure S4: Transient Bnc2 CRISPR/Cas9 Knockdown in Zebrafish Larvae Reproduces the Morpholino Phenotype

(**A**): Schematic showing the genomic positions of the different guide-RNAs used for the transient Bnc2 CRISPR/Cas9 targeting experiments.

(**B-C**): Single guide RNA (sgRNA) injections of guide 6 targeting *bnc2* with Cas9 reproduces the distal 'vesicle' as an outlet obstruction of the pronephric ducts in 5 % of injected embryos at 33 hpf (see inlays - black arrowheads). Kinked tails were observed in 1 % of the zfl (black asterisk).

(**D**): Follow-up of sgRNA injected zfl targeting *bnc2* for sgRNA 4 shows hydrocephalus (black asterisk) and light body curvature (black arrowheads) at 54 hpf.

(**E**): Kaplan-Meier plots for survival of acute multi sgRNA (mgRNA) approach for guides 2, 6 and 8 targeting *bnc2* with Cas9. Zfl were included in survival experiment after 24 hpf. Injected larvae show significantly ($p<0.0001$, Mantel-Cox test) reduced survival (median survival of 7 dpf) and 40 % survival at the end of the experiment.

Scale bars: 500 µm (B, C and D)

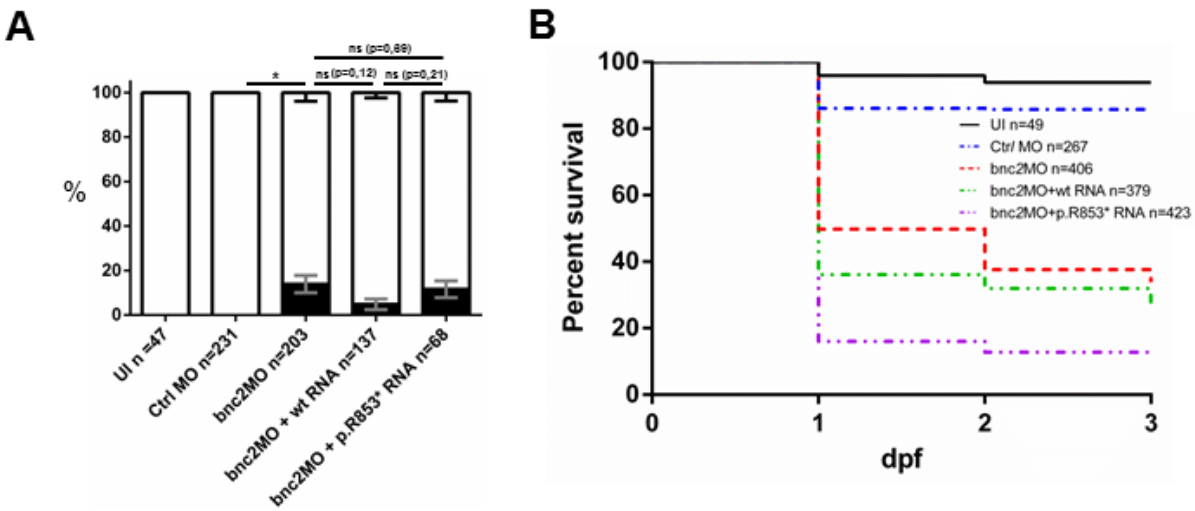
A
ns (p=0,89)
*
ns (p=0,12)
ns (p=0,21)
100
80
60
40
20
0
%
UI n =47
Ctrl MO n=231
bnc2MO n=203
bnc2MO + wt RNA n=137
bnc2MO + p.R853* RNA n=68
B
Percent survival
100
80
60
40
20
0
0
1
2
3
dpf
UI n=49
Ctrl MO n=267
bnc2MO n=406
bnc2MO+wt RNA n=379
bnc2MO+p.R853* RNA n=423

Figure S5: Co-injection of *bnc2* MO and Human Wildtype RNA in Zebrafish Larvae Results in a Reduced Formation of a Distal Pronephric Outlet Obstruction

(**A**): The graph shows 100 % of all at 1 dpf surviving zebrafish larvae (zfl) of the five different cohorts uninjected (UI), control Morpholino (Ctrl MO), *bnc*2 MO, *bnc2* MO + wildtype (wt) RNA (transcript ENST00000418777) and *bnc2* MO + mutated RNA bearing the p.R853* variant (for absolute numbers see Figure S5 A.) A distal 'vesicle' due to an outlet obstruction (phenotype) of the pronephric ducts can be seen in 14 % of *bnc2* MO injected zfl compared to 0 % of zfl with a 'vesicle' in both control groups ($p<0.05$, unpaired t-test). Zfl injected with *bnc2* MO + wt RNA develop a 'vesicle' in 5 %, injected with *bnc2* MO + p.R853* RNA in 11 %. * significance $p < 0.05$

(**B**): Quantification of death rates up to 3 dpf shows an increased mortality up to 66 % in *bnc2* MO injected zfl compared to UI (6 %) and Ctrl MO (14 %) injected zfl. Injected *bnc2* MO zfl show significantly ($p<0.0001$, Mantel-Cox test) reduced survival. Co-injection of *bnc2* MO + human wt RNA results in a mortality of 73 %. Aggravated mortality up to 88 % can be detected in the *bnc2* MO + p.R853* RNA injected zfl.

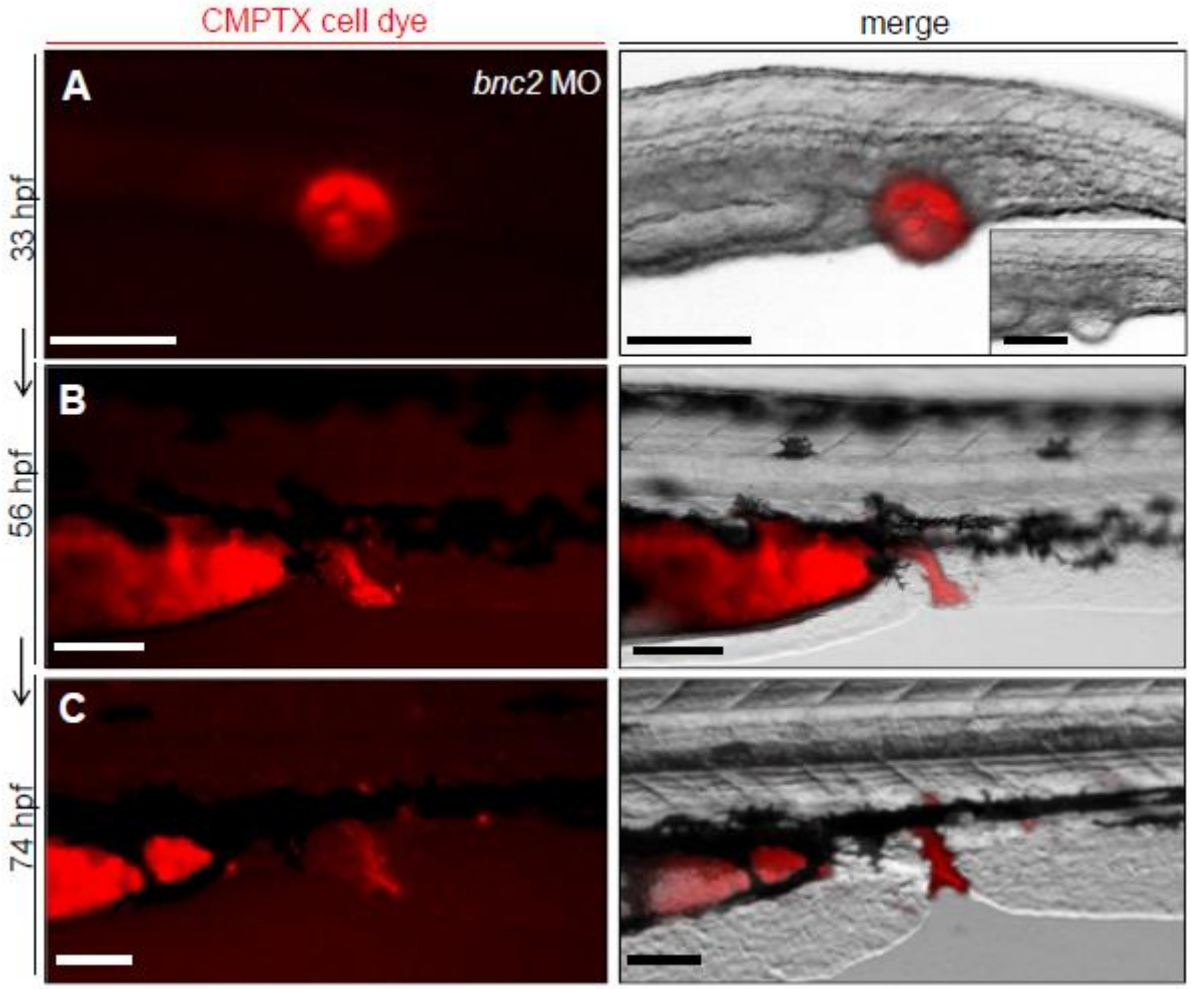
CMPTX cell dye
merge
A
bnc2 MO
B
C
33 hpf
56 hpf
74 hpf

Figure S6: Injection of Fluorescent Cell Dye Tracker CMTPX Indicates Surrounding Cells of Pronephric Outlet Obstruction to Later Form Parts of Distal Pronephric Ducts and the Cloaca

(**A-C**): Injection of fluorescent cell dye tracker CMPTX into the pronephric outlet obstruction ‘vesicle’ of a *bnc2* MO injected zebrafish embryo at 33 hpf and follow-up imaging of the same individual zebrafish demonstrates that cells forming the ‘vesicle’ become part of the distal end of the pronephric ducts and the cloaca later in development (56 and 74 hpf).

Scale bar: 100 μm (A, B and C)

Table S1: All Variants Segregating with Disease in Family 1 Identified by Exome Sequencing with a Frequency < 0.0001 According to gnomAD

	HGNC	RefSeq	Mutation cDNA	Mutation Protein	Allele frequency according to gnomAD
Loss of function variants					
ENST00000418777	*BNC2*	NM_001317939.1	c.2557C>T	p.Arg853*	0.000028
ENST00000295897	*ALB*	NM_000477.5	c.8G>A	p.Trp3*	*Novel*
Missense Variants					
ENST00000261405	*VWF*	NM_000552.3	c.7486C>A	p.Pro2496Thr	*Novel*
ENST00000397016	*CPNE6*	NM_006032.2	c.47C>T	p.Thr16Met	0.000009
ENST00000336395	*TESK1*	NM_006285.2	c.427T>G	p.Ser143Ala	*Novel*
ENST00000324001	*PRX*	NM_181882.2	c.1546C>T	p.Arg516Trp	0.000098
ENST00000372584	*HIVEP3*	NM_001127714.2	c.3611A>T	p.His1204Leu	0.000031
ENST00000311303	*ABCC12*	NM_033226.2	c.2957C>T	p.Pro986Leu	0.000008
ENST00000284061	*DGKE*	NM_003647.2	c.487G>A	p.Val163Ile	*Novel*
ENST00000295890	*COX18*	NM_173827.2	c.782G>A	p.Arg261His	0.00005
ENST00000378113	*C12orf42*	NM_198521.2	c.383G>C	p.Arg128Pro	*Novel*
ENST00000392839	*RIC8B*	NM_018157.2	c.1018G>C	p.Glu340Gln	0.000008
ENST00000278935	*CEP164*	NM_014956.4	c.4130C>T	p.Pro1377Leu	0.000083

Legend Table S2 (excel file):

[1] nucleotide, exon and amino acid numbering for *BNC2* is according to ENST00000380672.8; the cDNA position is according to the transcript with 5'UTR; IVS=intervening sequence (intron); [2] estimation of consensus splice site values (CVs) is according to Shapiro and Senapathy[6]; [3] ESS, exonic splice silencer; [4] ESE, exonic splice enhancer; threshold for: SRSF1, 1.956; SRSF1 (IgM-BRCA1), 1.867; SRSF2, 2.388: SRSF5, 2.67; SRSF6, 2.676

Supplemental Methods

Subject Ascertainment and Phenotypic Data of LUTO Re-sequencing Cohort

The study was conducted in adherence to the Declaration of Helsinki. The respective informed consent was obtained from the affected individuals or by proxies in the case of minors. The study was approved by the ethics committee of the medical faculty of the university of Bonn (No. 146/12) as well as the respective ethic committee of the collaborating centers in Boston, Manchester, Nijmegen (AGORA data and biobank). Pre- and postnatally diagnosed affected individuals were included in the cohort screened for mutations in *BNC2*. Prenatal inclusion criteria comprised the presence of a distended bladder with 'keyhole sign', and with vesicoureteral reflux including uni- or bilateral hydronephrosis of different degree. Postnatal diagnosis was made by the presence of a valve or stenosis at time of cystoscopy. Clinical data were obtained by direct sonographic or radiographic studies of all participants at the respective clinical centers or retrospective reviewing of the medical files from the respective treating physician.

For re-sequencing we used DNA of 697 individuals with LUTO. All of these 697 individuals with LUTO were of male gender. In 13 affected individuals with distended bladder pregnancy was aborted, exact origin of LUTO was not clarified. All other affected individuals presented postnatally with PUV, except for one individual who was described to have an anterior valve.

Variant Identification

Whole-exome sequencing was performed with genomic DNA extracted from peripheral blood, captured (Agilent SureSelect Human All Exon v5) and sequence data were

generated by a paired end 2 × 125 bp protocol on the Illumina HiSeq 2000. This resulted in a mean coverage of 80-fold, a 30x coverage of 91 %, and a 10x coverage of 98 % of target sequences. Scripts developed in-house at the Cologne Center for Genomics (CCG) were applied to detect protein changes, affected donor and acceptor splice sites, and overlaps with known variants. Acceptor and donor splice site mutations were analyzed with a Maximum Entropy model [1] and filtered for effect changes. In particular, we filtered for high-quality (minimal coverage >6; minimal quality >10) and heterozygous variants with a frequency below 0.0001 since we hypothesized an autosomal-dominant mode of inheritance. (dbSNP build 135, the 1000 Genomes database build 20110521, ExAc Browser Version 0.3.1, and the public Exome Variant Server, NHLBI Exome Sequencing Project, Seattle, build ESP6500). We also filtered against an in-house database containing variants from 511 exomes from individuals with epilepsy to exclude pipeline related artefacts (MAF<0.004). In a second step all remaining variants were checked for frequency in gnomAD version 2.0.2. Visual inspection of read quality was performed.

Re-sequencing of *BNC2* in Individuals with LUTO

Analysis of the human *BNC2* gene comprising 14 transcripts (ENST00000380672.8, ENST00000545497.5, ENST00000418777.5, ENST00000380667.6, ENST00000411752.5, ENST00000380666.6, ENST00000603713.5, ENST00000471301.3, ENST00000486514.5, ENST00000617779.1, ENST00000468187.6, ENST00000613349.4, ENST00000603313.5, ENST00000484726.5) listed in ‘ensembl database’ (www.ensembl.org/_September 30th 2017) was performed using Sanger Sequencing. PCR-amplified DNA products (primer

sequences available upon request) were subjected to direct automated sequencing using a 3130XL Genetic Analyzer (Applied Biosystems, Foster City, USA) according to the manufacturer's specifications, with PCR primers also served as sequencing primers.

Staining of Human Urethra

For our study, we have used the formalin-fixed paraffin embedded archive. Initially, tissues were fixed in the neutral buffered 4% formalin according to the institutional standards. Human embryonic material, collected with maternal consent and ethical approval (REC 08/H0906/21+5), was sourced from the MRC-Wellcome Trust Human Developmental Biology Resource (http://www.hdbr.org/).

Hematoxylin and Eosin (HE) Staining

All samples were stained by the hematoxylin and eosin (HE) method following the standard protocol. Sections of 3 µm thickness were obtained from the paraffin blocks. Subsequently, the sections were dewaxed in xylene, hydrated in solutions with decreasing concentrations of ethanol, stained, dehydrated in solutions with increasing concentrations of ethanol and mounted from xylene with pertex from Medite.

Immunohistochemistry Protocol

The tissue was cut (3 µm) and mounted on superfrost slides (Menzel Gläser, Brunswick). The immunohistochemical staining of the 3 µm cuts is performed on the fully integrated staining solution Benchmark Ultra from Roche/Ventana.

The slides were pretreated with CC1 (cell conditioning pH 8) (Roche Ultra-CCl, 950-224). Antibodies incubation time was 36 min at 37° C. We used mouse monoclonal Anti-BCN2 antibody, clone 2082C5a, Abcam 84845, dilution 1:50. The ultraView Universal DAB Detection Kit from Roche (760-500) was used. We used counterstaining with hematoxylin according to Mayer (3 min) then ascending alcohol series. The slides from xylene were mounted with pertex from Medite.

Immunohistochemistry Evaluation

The immunohistochemically staining was evaluated by two experienced pathologists. The staining intensity was evaluated using a 4-tier grading system (0: negative; 1: weakly positive; 2: moderately positive; 3: strongly positive) for membrane, nuclei and cytoplasm separately.

Mouse *In Situ* Hybridization and mRNA Sequencing

Presence of the different *Bnc2* mRNAs (*Bnc2-201* and *Bnc2-214*) in the urogenital region of the developing mouse embryo was verified by PCR. To this end, the urogenital region from three E12-5 mouse embryos was prepared and RNA extracted using the RNeasy Mini Kit (Qiagen) according to the standard protocol. 500ng of RNA was translated into cDNA using the QuantiTect Reverse Transcription Kit (Qiagen). The two transcript variants (*Bnc2-201*, ENSMUST00000102820.8 and *Bnc2-214*, ENSMUST00000176612.7) were detected with specific primers: *Bnc2-201*: forward: AAGAGATGCACGTCTGCACG, reverse: GTGTAGACACAGAGGCACACA; *Bnc2-214*: forward: ACAGAAACAGAAATTTACGGATGGA, reverse:

CGGAAGCACACACTGGCTAT. The obtained PCR products were sequenced for verification.

In situ probe generated by addition a 5' T7 polymerase transcriptional initiation sequence (aTAATACGACTCACTATAGGGG) to the reverse primer (*Bnc2-214* above). The ~800bp long PCR product was directly used for the antisense probe generation using the T7 RNA polymerase and a nucleotide mix containing digoxigenin-11-UTP (Roche Diagnostics). Following probe hybridization and washes, an Anti-DIG antibody conjugated to alkaline phosphatase (AP) (Roche) was incubated with embryos overnight at 4°C, and detection of AP activity was carried out using BM Purple (Roche).

Embryos were fixed overnight in 4% PFA and processed into paraffin wax. Sections were cut at a thickness of 5 µm. *In situ* hybridization was performed on paraffin sections (5 µm) according to the protocol from Chotteau-Lelievre et al. (2006) with minor modifications, and detection of alkaline phosphatase activity was visualized using BM Purple (Roche Diagnostics). Following staining, slides were quickly dehydrated in 80 % and then 100 % ethanol, cleared twice for 1 min in xylene (Roth) and coverslips were mounted with Entellan mounting medium (Merck). Images were captured using AxioVision software (Zeiss) with a Zeiss AxioCam. At least 2 embryos were analyzed and representative images taken.

Zebrafish (Zf) Lines and Maintenance

Zf were kept according to national law and to recommendations by Westerfield [2] in our fish facility in Bonn, Germany. Zf larvae of wild-type AB/TL and the transgenic strains

*Tg(wt1b:*eGFP*)* and *Tg(HGj4A)* were obtained by natural spawning and raised at 28°C on a 14 h light: 10 h dark cycle. Staging was performed according to Kimmel et al. [3].

Zf experiments with CRISPR/Cas9 were performed in Casper (*mitfa*$^{w2/w2}$*; mpv17*$^{a9/a9}$) at Boston Children's Hospital (BCH) Aquatic Core Facility. All national and institutional guidelines for the care and use of laboratory animals were followed. The zebrafish experiments were approved by the BCH Institutional Animal Care and Use Committee (IACUC).

Microinjections of Morpholino Oligonucleotides and mRNA

Embryos at the one-cell to two-cell stage were pressure injected into the yolk with Morpholino® oligonucleotide (MO) synthesized by GeneTools, LLC. Injections were carried out with 0.75 ng of *bnc2* MO (1.7nL/embryo) (5'-GAGCTTTCTCCTTCTTCTCCTCCTC -'3) and 0.75 ng of standard control MO (5'-CCTCTTACCTCAGTTACAATTTATA-'3). For human mRNA rescue experiments 30 - 100 pg of *in vitro* transcribed human *BNC2* mRNA was injected into the yolk of one-cell embryos. *BNC2* mRNA was transcribed from cDNA clone HsCD00399335 (Harvard Medical School) containing ENST00000380672.8 and from a custom-made cDNA clone (BioCat GmbH) containing ENST00000418777.5 using the mMESSAGE Machine T7 Kit (Ambion) and the Poly (A) Tailing Kit (Ambion) according to instructions.

Target Selection and sgRNA Generation

Single guide RNA (sgRNA) targets were selected using the CHOPCHOP online tool v1 following their ranking algorithm [4]and were generated by *in-vitro* transcription from

oligonucleotide based templates using the MEGAscript T7 Transcription Kit (Ambion). 2 µl of sgRNA stock (500 ng/µl) were mixed with 2 µl of recombinant Cas9 protein (1 µg/µl, PNA Bio, Thousand Oaks, CA) and incubated on ice for at least 10 min to allow formation of the sgRNA/Cas9 complex. 2 nl of the injection mix was injected intracellularly in one-cell stage zebrafish embryos. DNA was extracted and analyzed via Sanger sequencing to confirm mutagenesis. ICE synthego online tool was used to analyze sequences for insertions and/or deletions and for rate of mutagenesis (https://ice.synthego.com/#/).

Microinjections of Cell Tracer Dye CellTracker™ Red CMTPX

Tricaine (Sigma-Aldrich, Munich, Germany) at a concentration of 0.1–0.5 % (in 30 % Danieau's solution) was used to anesthetize larvae before microinjection of cell tracer dye CellTracker™ Red CMTPX (ThermoFisher Scientific) in the vesicle at a concentration of 5 uM. Larvae were consecutively imaged and kept up to 3 days post fertilization.

Western Blot Analysis

Zf samples were lysed in RIPA buffer with 4 % protease inhibitor, proteins separated by SDS-PAGE and transferred on PVDF membranes. Membranes were then incubated for several hours in blocking solution (5 % milk powder in TBST) before adding the anti-BNC2 primary antibody [2082C5a] in 1:1,000 dilution (Abcam) at 4°C overnight. After several washes in TBST the secondary HRP-goat anti-mouse antibody (Thermo Fisher Scientific) 1:10,000 dilution in blocking buffer was added for 1 hour at room temperature before imaging the membrane using enhanced chemiluminescent (ECL) HRP substrate for low-femtogram-level detection.

Whole-mount Zebrafish *In Situ* Hybridization (ISH)

Antisense and sense probes for *pax2a* were amplified from zebrafish poly-A embryonic cDNA and cloned in pBluescript. Antisense and sense probes for *bnc2* were amplified from cDNA clone IMAGE:7063814 (Source BioScience). Constructs were linearized by corresponding restriction enzymes and Dig-labelled RNA was synthesized using Roche Dig labelling kit. ISH was performed following instructions of Thisse et al., 2008[5].

Immunohistochemistry Staining of Whole-mount Zebrafish

Zebrafish larvae were euthanized using Tricaine (0.4–0.8 mg/ml) and fixed in 4% paraformaldehyde in PBS for 24h at 4°C. Samples were decalcified in 0.5 mM EDTA for 3 days at room temperature and embedded in paraffin according to standard procedures. Sections were obtained on a Leica RM2255 microtome (Leica Microsystems, Wetzlar, Germany). H&E staining was performed according to standard procedures. Immunohistochemical staining were performed with respective antibodies using Ventana Benchmark XT Automated IHC/slide staining system. Antibodies were used at the following dilutions. Anti-Cleaved caspase 3 (Cell signaling Technologies) 1:200 and Anti-BNC2 (Sigma) 1:200.

Imaging

At the stages of interest embryos were analysed under a Nikon AZ100 Macro-Zoom microscope and processed with NIS-Element Viewer software. Selected embryos were further anesthetized with 0.016 % tricaine, fixed in 2 % low-melting agarose and imaged

by two-photon scanning fluorescence in vivo microscope (LaVision Trim-ScopeII; Imspector and ImageJ software).

Statistical Analysis

Two-tailed Student's t-test, Mantel-Cox and two-way ANOVA test were used for analysis using GraphPad Prism version 6. Differences with a p-value of < 0.05 (*) were considered as being statistically significant.

Supplemental Web Resources

Human Splicing Finder, version 3.1 (www.umd.be/HSF3/)

ESE Finder, release 3.0 (http://krainer01.cshl.edu/cgi-bin/tools/ESE3/esefinder.cgi?process=home)

SFmap, version 1.8 (http://sfmap.technion.ac.il/)

Supplemental References

1. Yeo, G., and Burge, C.B. (2004). Maximum entropy modeling of short sequence motifs with applications to RNA splicing signals. J. Comput. Biol. J. Comput. Mol. Cell Biol. *11*, 377–394.

2. Westerfield, M. (2000). The zebrafish book. A guide for the laboratory use of zebrafish (Danio rerio). (Eugene: Univ. of Oregon Press).

3. Kimmel, C.B., Ballard, W.W., Kimmel, S.R., Ullmann, B., and Schilling, T.F. (1995). Stages of embryonic development of the zebrafish. Dev. Dyn. Off. Publ. Am. Assoc. Anat. *203*, 253–310.

4. Montague, T.G., Cruz, J.M., Gagnon, J.A., Church, G.M., and Valen, E. (2014). CHOPCHOP: a CRISPR/Cas9 and TALEN web tool for genome editing. Nucleic Acids Res. *42*, W401-407.

5. Thisse, C., and Thisse, B. (2008). High-resolution in situ hybridization to whole-mount zebrafish embryos. Nat. Protoc. *3*, 59–69.

6. Shapiro, M.B., and Senapathy, P. (1987). RNA splice junctions of different classes of eukaryotes: sequence statistics and functional implications in gene expression. Nucleic Acids Res. *15*, 7155–7174.